DMD Fast Forward. Published on April 20, 2016 as DOI: 10.1124/dmd.116.069542
This article has not been copyedited and formatted. The final version may differ from this version.

DMD #69542

Metabolite Kinetics: The Segregated-Flow Model (SFM) for Intestinal and Whole Body PBPK Modeling To Describe Intestinal and Hepatic Glucuronidation of Morphine in Rats *In Vivo*

Qi J. Yang, Jianghong Fan, Shu Chen, Lutan Liu, Huadong Sun, and K. Sandy Pang,

Department of Pharmaceutical Sciences, Leslie Dan Faculty of Pharmacy, University of Toronto (QJY, JF, SC, LL, HS, KSP)

Present Address:

Office of Generic Drugs, Food and Drug Administration, Silver Springs, MD, USA (JF)

Apotex Inc., Toronto, Ontario, Canada (SC)

Bristol Myers Squibb, Princeton, New Jersey, USA (HS)

DMD Fast Forward. Published on April 20, 2016 as DOI: 10.1124/dmd.116.069542
This article has not been copyedited and formatted. The final version may differ from this version.

Running Title: SFM for intestinal morphine glucuronidation

Send inquiries and reprint requests to

Dr. K. Sandy Pang
Leslie Dan Faculty of Pharmacy
University of Toronto
144 College Street
Toronto, Canada M5S 3M2
TEL: 1-416-978-6164
FAX: 1-416-978-8511
Email: ks.pang@utoronto.ca

Abstract: 248

Introduction: 748

Discussion: 1480

References: 57

Figures: 6

Tables: 8

Abbreviations: M, morphine; MG, morphine glucuronide; A_{urine}^{MG} , cumulative amount of MG in urine; A_{bile}^{MG} , cumulative amount of MG in bile; IV, intravenous; ID, intraduodenal; PO, oral; TM, traditional model; SFM, segregated flow model ; PBPK, physiologically-based pharmacokinetic model

DMD Fast Forward. Published on April 20, 2016 as DOI: 10.1124/dmd.116.069542
This article has not been copyedited and formatted. The final version may differ from this version.

ABSTRACT

We used the intestinal segregated flow (SFM) vs. the traditional (TM) model, nested within physiologically-based pharmacokinetic (PBPK) models, to describe the biliary and urinary excretion of morphine 3β-glucuronide (MG) after intravenous and intraduodenal dosing of morphine in rats *in vivo*. The SFM model describes a partial (5-30%) intestinal blood flow perfusing the transporter- and enzyme-rich enterocyte region whereas the TM describes 100% flow perfusing the intestine as a whole. For the SFM, drugs entering from the circulation are expected to be metabolized to lesser extents by the intestine due to the segregated flow, reflecting the phenomenon of shunting and route-dependent intestinal metabolism. The poor permeability of MG crossing the liver or intestinal basolateral membranes mandates that most of MG that is excreted into bile is hepatically formed, whereas MG that is excreted into urine originates from both intestine and liver metabolism, since MG is effluxed back to blood. The ratio of MG amounts in urine/bile ($\frac{A_{urine}^{MG}}{A_{bile}^{MG}}$) for intraduodenal/intravenous dosing is expected to exceed unity for the SFM but approximate unity for the TM. Compartmental analysis of M and MG data, without consideration of the permeability of MG and where MG is formed suggests the ratio to be 1, and failed to describe the kinetics of MG. The observed intraduodenal/intravenous ratio of $\frac{A_{urine,4h}^{MG}}{A_{bile,4h}^{MG}}$ (2.55 at 4 h) was better predicted by the SFM-PBPK (2.59 at 4 h) and not the TM-PBPK (1.0), supporting the view that SFM is superior for the description of intestinal-liver metabolism of morphine to MG.

DMD Fast Forward. Published on April 20, 2016 as DOI: 10.1124/dmd.116.069542
This article has not been copyedited and formatted. The final version may differ from this version.

INTRODUCTION

It has been recognized that, generally, compartmental modeling is unable to quantitatively address the multiplicity of metabolite formation organs nor account for sequential metabolism/excretion or permeability barriers of formed metabolites (Pang et al., 2008; Pang, 2009). In contrast, physiologically-based pharmacokinetic (PBPK) models address events of sequential elimination and includes transmembrane barriers (deLannoy and Pang, 1986; 1993; Pang, 2003; Pang et al., 2009; Chow and Pang, 2013) and transporters (Sun et al., 2006: Sun et al., 2010). The intestine, richly endowed with enzymes and transporters (van Herwaarden et al., 2007; Zhang et al., 2007, 2009; Liu et al., 2010), strongly impacts first-pass metabolism and controls the flow of substrate to the liver (Pang and Chow, 2012). Intestinally formed metabolites may undergo immediate sequential metabolism or secretion (Pang and Gillette, 1979). When the metabolite possesses good permeability or transporter-linked properties, it will cross the liver cell membrane to endure liver metabolism and/or biliary excretion prior to reaching the lung, heart, and the general circulation.

Route-dependent metabolism by the intestine is repeatedly being observed, namely, a higher extent of intestinal metabolism exists when a drug is given orally vs. the lower extent or virtual absence of intestine metabolism when given systemically (Doherty and Pang, 2000; Cong et al., 2000; Fan et al., 2010). This was observed for erythromycin (Lown et al., 1995) and midazolam (Paine et al., 1996) in man, and enalapril hydrolysis (Pang et al., 1985) and morphine glucuronidation in the rat intestine (Doherty and Pang, 2000). The lesser extent of intestinal metabolism for systemically-delivered drug is explained by the pattern that a fraction and not the entire intestinal blood flow perfuses and recruits enzymes/excretory transporters in the enterocyte

region, with the majority of flow perfusing the inactive, serosal region (Cong et al., 2000; Fan et al., 2010). These observations led to the development of the segregated flow model (SFM), describing that only a partial intestinal flow (5-30%) reaches the enterocyte region to explain the higher oral vs. intravenous (IV) intestinal metabolism. In contrast, the traditional model (TM) describes no difference, since the entire intestinal flow perfuses the intestinal tissue as a whole (Cong et al., 2000).

In this study, we examined morphine glucuronidation in the rat *in vivo* after administration of small doses of M (or natural (-)-morphine) in saline into the jugular vein for IV or duodenal lumen (or intraduodenal, ID) dosing, with continuous bile collection *via* a catheter. We studied M, which enters the cell by passive diffusion (Doherty et al., 2006) and is primarily glucuronidated at the 3-position to form morphine 3β-glucuronide (MG) by Ugt2b1 in the rat intestine and liver (Rane et al., 1985). Morphine is also known to be metabolized by Cyp/CYP (Projean et al., 2003) and undergoes excretion *via* the P-gp (Böerner 1975; Iwamoto and Klaassen, 1977; Letrent et al., 1999; Wandel et al., 2002) to minor extents. The rat kidney actively secretes but does not metabolize M (Van Crugten et al., 1991; Shanahan et al., 1997). MG is excreted from formation tissues; enterohepatic circulation in rats has been noted (Dahlström and Paalzow, 1978; Horton and Pollack, 1991) but not for the rat with an open bile fistula. The influx permeability of MG through the liver (0.1 $mL \cdot min^{-1} \cdot g^{-1}$ liver) was estimated to be 5-10% of the flow rate, suggesting the existence of a diffusional barrier for MG to enter the hepatocyte (Doherty et al., 2006). Intestinally formed MG undergoes luminal secretion via Mrp2 and is effluxed into the circulation via Mrp3 in the rat (van de Wetering et al., 2007). MG formed in liver is biliarily excreted as well as effluxed out. These MG species of intestinal and hepatic origins that reenter the circulation are

DMD Fast Forward. Published on April 20, 2016 as DOI: 10.1124/dmd.116.069542
This article has not been copyedited and formatted. The final version may differ from this version.

excreted by the kidney, with clearance values that are similar to the glomerular filtration rate (Van Crugten et al., 1991). Intuitively speaking, the extents of intestine vs. liver formation of MG, reflected by their appearance in urine/bile, should remain the same for both intravenous and ID dosing, when the flow patterns for the delivery of M to the intestine and liver are the same for different routes of drug administration, as with the TM model. By contrast, when M in the systemic circulation is being partially shunted away from the enterocyte for metabolism with IV dosing for the SFM model, the urine/bile ratio of MG for IV dosing of M is expected to be lower than that for ID. The different extents of excretion of MG in bile vs. urine for ID vs. IV dosing of M could be used to appraise which intestine model, TM or SFM, best describes first-pass metabolism when nested within PBPK models.

DMD Fast Forward. Published on April 20, 2016 as DOI: 10.1124/dmd.116.069542
This article has not been copyedited and formatted. The final version may differ from this version.

MATERIALS AND METHODS

Materials

Natural (-)-morphine (M), and morphine 3β-glucuronide (MG) were provided by the National Institutes on Drug Abuse (NIDA, Rockville, MD, USA); caffeine (internal standard) was purchased from Sigma-Aldrich Co. (St. Louis, MO, USA). HPLC grade acetonitrile, methanol and formic acid were obtained from Fisher Scientific Canada (Ottawa, ON). Male Sprague-Dawley rats (St Constant, QC), weighing 305 ± 10 g (age 8-9 weeks), were used throughout the study.

In vivo pharmacokinetic study

Rats were maintained under constant housing and environmental conditions (temperature, lighting, and diet) according to protocols approved by the University of Toronto. Rats were abstained from food but given 5% w/v glucose water overnight before the day of study. Pentobarbital (65 $mg \cdot kg^{-1}$ intraperitoneally, IP) was used to induce anesthesia since ketamine was reported to inhibit morphine glucuronidation (Qi et al., 2010). Under anesthesia, the carotid artery was cannulated with PE50 tubing, which was pre-filled with heparinized (1000 U/ml) physiologic saline solution for sampling; the contralateral jugular vein was cannulated for the IV administration of M (Hirayama et al., 1990). The ID dose solution was introduced as a bolus needle-injection into the proximal duodenum. A midline incision was made for bile duct cannulation with PE50 tubing. The opened neck and abdominal regions for the surgical manipulations were sutured immediately after drug administration. For intravenous (IV) administration, natural (-)-morphine (M) (expressed as morphine base, 14.9±1.6 $\mu mole \cdot kg^{-1}$ in 0.2 ml saline solution) was administered as a bolus into the jugular vein, followed by flushing of the

DMD Fast Forward. Published on April 20, 2016 as DOI: 10.1124/dmd.116.069542
This article has not been copyedited and formatted. The final version may differ from this version.

inline contents with saline. For ID administration, morphine sulfate (expressed as M, 26.6 ± 0.40 μmole·kg^{-1} in 0.3 ml saline solution) was injected into the proximal duodenal lumen. The difference in weights of the syringe before and after the injection was taken as the volume of dose injected, and the dose solution was assayed by LC/MS. Blood (0.1 ml) was collected via the carotid artery cannula of the same rat at 0, 1, 5, 10, 15, 30, 45, 60, 90, 120, 180, and 240 min after dosing for each rat. Bile was collected *in toto via* the bile duct cannula at 0, 5, 10, 15, 20, 30, 45, 60, 90, 180 and 240 min after dosing into pretared 1.5 ml vials. At the end of study (240 min), the entire urinary content was collected from the bladder via sampling with a needle/syringe. All samples were kept frozen at -20ºC until analysis.

LC/MS/MS assay: protein precipitation, solid phase extraction (SPE)

A set of standards of known, added amounts of M and MG in blood was processed in the same manner as the samples. Caffeine, the internal standard (10 μL of 3 μg·mL^{-1}) was added to 100 μL blood, followed by protein precipitation with 400 μL of an equimixture of methanol and acetonitrile, which was found to yield the highest recovery of the compounds. After vortex-mixing for 60 s and centrifugation at 13,000×g for 10 min, the supernatant was transferred into Sep-Pak Vac C_{18} 3 cc cartridges (200 mg; Waters, Milford, MA, USA). Each cartridge was pre-conditioned with 2×1 mL of acetonitrile followed by 2×1 mL Millipore water. After loading of sample, 0.5 mL 5% acetonitrile in water was added into the cartridge and the contents in the cartridge were eluted with 2×1 mL acetonitrile. The eluent was pooled and dried under N_2 at room temperature. The residue was reconstituted with 200 μL of the mobile phase (70% of water with 0.1%v/v formic acid and 30% acetonitrile with 0.1%v/v formic acid), and 5 μL of the reconstituted sample was injected into the LC–MS/MS system.

DMD Fast Forward. Published on April 20, 2016 as DOI: 10.1124/dmd.116.069542
This article has not been copyedited and formatted. The final version may differ from this version.

Calibration curves for the quantification of M and MG in bile and urine samples were constructed under identical conditions. Due to the differential abundances of MG and M in bile, 10 μL (for MG assay) and 40 μL (for morphine assay) bile were assayed in separate analyses. Samples were spiked with 5 or 10 μL of the IS solution, then diluted with saline to 100 μL, before mixing with 400 μL of methanol and acetonitrile (1:1 v/v) for SPE loading. For urine analysis, 10 μL of the urine sample was spiked with 10 μL of the IS solution and diluted to 100 μL with saline, then mixed with 400 μL of methanol and acetonitrile (1:1 v/v) for SPE loading. These samples were then processed identically to that described for the blood samples.

LC–MS/MS. The LC–MS/MS was comprised of an Agilent 1200 series LC coupled to an Agilent 6410 triple-quadruple MS with an electrospray source (Santa Clara, CA). A HPLC gradient consisting of the mobile phase components of 0.1% formic acid in water (A) and 0.1% formic acid in acetonitrile (B), increasing from 4% to 30% between 5 to 10 min, then returning to 4% over the next min, was developed to separate MG, morphine, and caffeine (IS) at retention times of 2.6, 4.3, and 10.9 min, respectively. Transitions from precursor ion to product ion were observed with MRM (multiple reaction monitoring): MG (m/z 462 → 286), morphine (m/z 286.1 → 165), and caffeine (m/z 195 → 138). Fragments or voltage (Frag) and collision energy (CE) were: for MG, Frag 160 V, CE 32 V; for M, Frag 165 V, CE 40 V; for caffeine, Frag 85 V, CE 24 V. The area of each peak, obtained by the MassHunter workstation software (Agilent Technologies), was normalized to that of the IS. A good correlation that showed linearity ($R^2 > 0.997$) between the added compound/I.S. area ratio vs. amount of compound in sample (blood/bile/urine) was observed. The coefficient of variation was < 14% for all the concentrations studied. The intraday

DMD Fast Forward. Published on April 20, 2016 as DOI: 10.1124/dmd.116.069542
This article has not been copyedited and formatted. The final version may differ from this version.

CV was between 0.4 to 9.2% for M concentrations ranging between 20 to 2470 ng·mL^{-1}, and 0.9 to 12.9% for MG for concentrations ranging between 16 to 2390 ng·mL^{-1}. The data showed good linearity for the blood (R^2>0.997), urine (R^2>0.98) and bile (R^2>0.98) calibration curves, and the LOQ for morphine and MG were 9.75 and 19.5 ng·mL^{-1}, respectively.

Data analysis

Noncompartmental/Compartmental analyses

The total AUC_{∞} [area under the concentration-time curve to infinity] was estimated as sum of $AUC_{0\text{-}t}$, obtained with the trapezoidal rule, and AUC_{extrap}, obtained by dividing the blood concentration of the last sampling point (C_{last}) by β, the terminal slope. The total body (blood) clearance (CL_{tot}) was calculated as $Dose_{IV}/AUC_{\infty,IV}$. The bioavailability or F_{sys} was calculated from the dose-normalized $AUC_{\infty,ID}/AUC_{\infty,IV}$ or approximated by the amounts of M excreted into urine at 4 h after ID/IV dosing. Concentration and amount data were normalized to dose, and data were expressed mean ± SD.

A two compartment model for M and a one compartment model for MG were used for compartmental analysis and fitting of M and MG data (Fig. 1). The total elimination rate constant of M arising from the central compartment (k_{10}) comprises of the metabolic (k_m), biliary (k_{bile}), renal (k_{renal}) excretion rate constant, and $k_{m,others}$ for other metabolic pathways; and k_a, k_{12} and k_{21} denote the absorption and intercompartmental rate constants, respectively; V_1 and F_{sys} are the central volume of distribution and bioavailability, respectively. The metabolite, MG, with volume of distribution V{mi}, is excreted into bile and urine, with rate constants, $k\{mi\}_{bile}$ and $k\{mi\}_{renal}$, respectively.

DMD Fast Forward. Published on April 20, 2016 as DOI: 10.1124/dmd.116.069542
This article has not been copyedited and formatted. The final version may differ from this version.

PBPK Models. The TM-PBPK and SFM-PBPK models (Fig. 2) were used for optimization of the IV and ID blood, bile and urine data of M and MG. Five tissues: rapidly perfused (RP), poorly perfused (PP) and adipose (AD) tissue, liver (L) and intestine (I) that are denoted as subscripts and interconnected by blood flow (Q), were considered. For detailed consideration of first-pass metabolism of M, the liver and intestinal tissues were subcompartmentalized as the tissue and tissue blood compartments to better accommodate the permeability barrier of MG. M in intestine blood (IB) and liver blood (LB) rapidly exchanges with those in tissue with influx ($CL^{M}_{in,I}$ and $CL^{M}_{in,L}$, high values) and efflux ($CL^{M}_{ef,I}$ and $CL^{M}_{ef,L}$, high values) clearances, respectively. In liver, M forms MG and other metabolites with intrinsic clearances, $CL^{M\rightarrow MG}_{int,met,L,}$ and $CL^{M\rightarrow others}_{int,met,L,}$, respectively, or is biliarily excreted ($CL^{M}_{int,sec,L}$). The MG formed in the intestine and liver is either effluxed out with $CL^{MG}_{ef,I}$ and $CL^{MG}_{ef,L}$ or secreted into the intestinal and bile canaliculus with secretory intrinsic clearances, $CL^{MG}_{int,sec,I}$ and $CL^{MG}_{int,sec,L}$, respectively. MG does not enter the intestine (Doherty and Pang, 2000) but is able to enter the liver, albeit with low permeability (0.1 $mL\cdot min^{-1}\cdot g^{-1}$ liver) (Doherty et al., 2006). The hepatic, influx clearance of MG into liver ($CL^{MG}_{in,L}$) was hence assigned (0.1 $mL\cdot min^{-1}\cdot g^{-1}$ liver) (Fig. 2). For simplification, the renal excretion of M and MG from the kidney occurs from the central compartment with renal clearances, CL^{M}_{R} and CL^{MG}_{R}, respectively. For the SFM, the intestine tissue is further subdivided into the enterocyte (en) and serosal (s) regions and the corresponding blood regions (enB and sB); the enterocyte flow, Q_{en}, perfusing the metabolically active and transporter-rich region is only a small fraction (f_Q = 0.05 to 0.3) of the total intestinal flow rate, Q_I or Q_{PV}; the serosal flow, Q_s, is $(1\text{-}f_Q)Q_I$ (Fig. 2B) (Cong et al., 2000).

DMD Fast Forward. Published on April 20, 2016 as DOI: 10.1124/dmd.116.069542
This article has not been copyedited and formatted. The final version may differ from this version.

Fitting. Fitting was conducted by the ADAPT 5 Systems Analysis Software (BMSR Biomedical Simulations Resource, USC, Version 5, Los Angeles, CA). The population method and the maximum likelihood with EM algorithm (MLEM) were used to fit individual sets of data (IV, n=4; ID, n=3) and the population data set that is based on individual data sets. We employed a two compartment model for M and a one compartment model for the metabolite, MG, to fit individual data sets (data for each rat) and all of the data as a whole (Fig. 1). Fitted results furnished estimates of k_a, total elimination (k_{10}), k_m, k_{bile}, k_{renal}, k_{others}, k_{12}, k_{21}, V_1, and F, with rate equations shown in Appendix A.

Then the TM-PBPK and SFM-PBPK models (Fig. 2) were used for fitting, with assigned physiological volumes and flows that are obtained from literature values and summarized in Table 1. The transport clearances for M ($CL^M_{in,I}$, $CL^M_{ef,I}$, $CL^M_{in,L}$, and $CL^M_{ef,L}$) were first assigned as 5x flow to tissue; the tissue to blood partitioning coefficients of M for the rapidly perfused (K_{RP}), poorly perfused tissue (K_{PP}), and adipose tissue (K_{AD}), calculated according to Rodgers and Rowland (2006; 2007), were used as initial estimates (Table 2) and the parameters were optimized by fitting. Similar K_T values for MG were not needed since transport terms were used for the intestine and liver, the few tissues where MG was distributed. The equations, assumptions and mass balance equations are shown in the Appendix B. Only the unbound species was involved in transport and elimination; the unbound fraction in plasma (f_P) was corrected by the blood/plasma concentration ratio (C_B/C_P) to obtain the unbound fraction in blood, f_B. The tissue unbound fraction (f_T) and the intrinsic metabolic or transport clearance was estimated as a combined estimate. All of the intrinsic clearances for metabolism ($CL_{int,met}$) and secretion ($CL_{int,sec}$) for the intestine (I) and liver (L), as well as the rate constants for absorption (k_a) and luminal degradation (k_g) and fraction of dose absorbed in gut lumen, F_{abs}, were obtained by fitting.

DMD Fast Forward. Published on April 20, 2016 as DOI: 10.1124/dmd.116.069542
This article has not been copyedited and formatted. The final version may differ from this version.

We also fitted the data with the nested TM- and SFM-PBPK models. With the fitted constants, simulations were extended to time infinity to estimate the amounts of MG in bile and urine for the TM- or SFM-intestine compartment nested in the PBPK model. Ratios of amounts of MG excreted into urine and bile after ID and IV dosing of M were then compared for the TM- and SFM-PBPK models.

The final model was selected based on the goodness-of-fit criteria, which included convergence, parameter precision, and visual inspection of predicted versus observed values and residual plots. The sum of squared residuals, coefficient of variation (CV or standard deviation of fitted parameter/parameter estimate), residual plots, as well as the F test were used to compare goodness of fit of the nested TM- and SFM-PBPK models (Boxenbaum *et al.*, 1974).

Mass balance solutions for M and MG amounts in bile and urine

Simple mass balance considerations were developed to illustrate the relationship between the intestine and liver in forming the metabolite in question. It was assumed that the intestine and liver are the only two organs capable of forming MG, and M is completely absorbed. For simplification, MG is assumed unable to enter the intestine or liver. Mass balance relations involving the intestinal and hepatic availabilities/extraction ratios of M and MG, the formed metabolite, are included to describe the formation of MG by the intestine and liver, and in the sequential removal of MG after its formation.

Statistical Comparisons

The two-tailed Student's *t* test was used to compare the means, and a *P* value of <.05 was viewed as significant.

DMD Fast Forward. Published on April 20, 2016 as DOI: 10.1124/dmd.116.069542
This article has not been copyedited and formatted. The final version may differ from this version.

RESULTS

In vivo pharmacokinetics of M after IV and ID dosing to rats – noncompartmental analysis. M decayed biexponentially after IV dosing, although the biphasic profile was not apparent after ID dosing (Fig. 3). The terminal half-lives for M, estimated by regression of log linear portion of decay curves, were identical for ID and IV dosing (61 and 67 min; $P > .05$). The area under the blood concentration-time curve for M ($AUC_{\infty,IV}$), obtained by summing the AUC by the trapezoidal rule and extrapolated area (C_{last}/β), yielded a total body blood clearance (CL_{tot}) of 6.6 ± 3.3 mL·min^{-1}, a value comparable to the blood clearance of 6.31 mL·min^{-1} [$CL_P/(C_B/C_P)$ according to Mistry and Houston (1987), based on plasma clearance, CL_P, of 8.46 and C_B/C_P ratio of 1.34]. Both M and MG were recovered in bile and urine in different proportions (Table 3; Fig. 3). The renal clearance of M, approximated by $\left(\frac{A^{M}_{urine,4h,IV}}{AUC^{M}_{0\text{-}4h,\,IV}}\right)$, was 2.21 mL·min^{-1}, and the unbound renal clearance was 2.6 mL·min^{-1} after correction for the plasma unbound fraction, a value similar to the glomerular filtration rate of 1.01 mL·min^{-1} per 100 g rat, as found with ^{125}I-iothalamat infusion (de Vries et al., 1997). The bioavailability (F_{sys}) estimated according to the dose-corrected $AUC_{\infty,ID}/AUC_{\infty,IV}$ and ID/IV ratio of amounts of morphine recovered in urine at 4 h, were 0.229 and 0.215, respectively (Table 3). These values are lower than that (0.33-0.36) from Mistry and Houston (1987) but slightly higher than those (0.14 and 0.15) reported by Iwamoto and Klaassen (1977) and Dahlström and Paalzow (1978).

MG appeared rapidly in blood, and the terminal half-lives (79 and 72 min) of decay of MG from IV and ID dosing of M were slightly but insignificantly longer than those for M ($P > .05$; paired *t*, Table 3). The area under the curve (AUC) for MG after ID dosing of M was 2x that of IV,

DMD Fast Forward. Published on April 20, 2016 as DOI: 10.1124/dmd.116.069542
This article has not been copyedited and formatted. The final version may differ from this version.

showing that use of metabolite AUC^{MG} for ID/IV would not reflect the systemic availability. The renal clearance of MG, approximated by $\frac{A^{MG}_{urine,4h,IV}}{AUC^{MG}_{4h,IV}}$, was 2.63 mL·min^{-1}, and was 2.68 mL·min^{-1} after correction for the unbound fraction in plasma (0.98); the value is slightly lower than the GFR of de Vries et al. (1997). The %dose of MG in bile at 4 h ($A^{MG}_{bile,4h}$ / Dose) was 80% higher for ID than with IV dosing, whereas the %dose of MG recovered in urine at 4 h ($A^{MG}_{urine,4h}$ / dose) for ID dosing was 4.65-fold that for the IV dose (Table 3). As a result, the $\frac{A^{MG}_{urine,4h,ID}}{A^{MG}_{bile,4h,ID}}$ ratio was 2.55*x* that of $\frac{A^{MG}_{urine,4h,IV}}{A^{MG}_{bile,4h,IV}}$ at 4 h after dosing (Table 3).

Compartmental modeling of M and MG. Fitting of the blood concentration-time profiles of M and MG following IV and ID dosing was generally satisfactory for both IV and ID dosing (Fig. 3). However, MG in bile was overestimated for IV but underestimated for ID data, whereas MG in urine was overpredicted for IV but underpredicted for ID dosing. The AUCs provided an estimate of 0.95 for F_{abs} that was higher than observed. The calculated, total clearance ($k_{10}V_1$) was 0.0711* 140 or 9.95 mL·min^{-1} (Table 4) and was higher than that observed (Table 3). According to the ratio of each rate constant/k_{10}, the pathways for formation of other metabolites (1.4%), and the biliary (less than 1%) and renal (31%) excretion contributed much less to the total elimination compared to the glucuronidation pathway (67.5%) or k_m/k_{10}.

SFM-PBPK and TM-PBPK modeling of M and MG. The tissue/blood partitioning ratios were calculated based on the methods of Rodgers and Rowland (2006; 2007) with use of known fractional volumes of the intracellular and extracellular tissue water, and neutral lipid and

DMD Fast Forward. Published on April 20, 2016 as DOI: 10.1124/dmd.116.069542
This article has not been copyedited and formatted. The final version may differ from this version.

phospholipid, and concentration of binding elements: extracellular albumin, acidic phospholipids, and neutral lipids and phospholipids; the pKa and the oil to water partition coefficient, $P_{o/w}$ for octanol:water and vegetable oil:water, were used in the calculation. These were compared to the optimized tissue to blood partitioning coefficients (K_T) that were estimated by fitting (Table 2). Generally, the fitted estimates were within $\pm$ 2-fold of the calculated values of K_{RP}, K_{PP} and K_{AD}.

The fits to the PBPK models are much improved compared to that from compartmental fitting (compare Figs. 3 and 4; Table 6). The blood levels of MG were less well predicted by the TM than for the SFM; MG appearance was overestimated in bile both after IV and ID dosing but underestimated in urine after ID dosing by TM. Pictorially, predictions by the SFM-PBPK model provided data that closely matched the observed, temporal data for concentration, bile, and urinary profiles up to the 4 h, in comparison to the TM (Fig. 4). The fitted parameters of the SFM-PBPK and TM-PBPK are summarized in Table 5. The predicted vs. observed data (Figs. 5 and 6) showed that the SFM-PBPK model fitted the data better than the TM-PBPK model. The F test showed that the SFM-PBPK provided the best fits over those for TM-PBPK and the compartmental model (Table 6).

Additional parameters were obtained from PBPK modeling (Table 7). The apparent (unbound) tissue to blood partitioning ratio of M, obtained from the ratio $\frac{f_B^M CL_{in,I}^M}{f_I^M CL_{ef,I}^M}$ and $\frac{f_B^M CL_{in,L}^M}{f_L^M CL_{ef,L}^M}$ are 0.14 to 0.53 for the intestine and 1.4 to 2.5 for the liver for the TM- and SFM-PBPK models. We estimated F_I and F_L as $\frac{CL_{ef,I}^M}{CL_{ef,I}^M + CL_{int,sec,I}^M(1-F_{abs}) + CL_{int,met,I}^{M\to MG}}$ and $\frac{CL_{ef,L}^M}{CL_{ef,L}^M + CL_{int,met,L}^{M\to MG} + CL_{int,met,L}^{M\to others} + CL_{int,sec,L}^M}$,

DMD Fast Forward. Published on April 20, 2016 as DOI: 10.1124/dmd.116.069542
This article has not been copyedited and formatted. The final version may differ from this version.

respectively, or with F_I and F_L as $\frac{f_Q Q_I CL^M_{ef,I}}{f_Q Q_I CL^M_{ef,I} + (f_Q Q_I + f_B^M CL^M_{in,I})\left[CL^{M\rightarrow MG}_{int,met,I} + CL^M_{int,sec,I}(1-F_{abs})\right]}$ and $\frac{(Q_I + Q_{HA})(CL^M_{ef,L} + CL^M_{int,sec,L} + CL^{M\rightarrow MG}_{int,met,L} + CL^{M\rightarrow others}_{int,met,L})}{(Q_I + Q_{HA})(CL^M_{ef,L} + CL^M_{int,sec,L} + CL^{M\rightarrow MG}_{int,met,L} + CL^{M\rightarrow others}_{int,met,L}) + f_B^M CL^M_{in,L}(CL^M_{int,sec,L} + CL^{M\rightarrow MG}_{int,met,L} + CL^{M\rightarrow others}_{int,met,L})}$ according to the equations of Sun and Pang (2010). These F_I values were 0.65 and 0.63 for TM and 0.46 and 0.28, respectively for the SFM; the F_L were 0.57 and 0.71 for TM and 0.58 and 0.72, respectively for the SFM (Table 7). The calculated F_I values for TM and SFM were slightly different with both methods of estimation, with the latter F_I values being influenced by f_Q. By contrast, F_L values were similar regardless of the equation used. For MG that is formed in tissue, the availability or fraction that escapes into the circulation, $F\{mi\}_I$ or $\frac{CL^{MG}_{ef,I}}{CL^{MG}_{ef,I} + CL^{MG}_{int,sec,I}}$ was 0.95 and 0.89 for the intestine, whereas $F\{mi\}_L$ or $\frac{CL^{MG}_{ef,L}}{CL^{MG}_{ef,L} + CL^{MG}_{int,sec,L}}$ was 0.11 to 0.22 for the liver, for the TM- and SFM-PBPK models. The fraction of hepatic clearance of M forming MG, or h_{mi}, was obtained as ratio of the formation intrinsic clearance/total intrinsic clearance, or >85% for both TM- and SFM-PBPK models, showing that glucuronidation is a major elimination pathway in the liver. The fraction of total body clearance of M forming MG, g_{mi}, was around 57 to 63 %, a value similar to the estimate from the compartmental model. The value is lower since M is excreted unchanged into urine.

The fractional contributions of the intestine and liver to the first-pass removal were estimated. The extents of intestine and liver removal of M are highly dependent on f_Q, the fractional enterocyte flow (Pang and Chow, 2012):

$$\frac{v_I}{v_I + v_L} = \frac{f_Q Q_I (1-F_I)}{f_Q Q_I (1-F_I) + E_L \left\langle Q_I \left[f_Q F_I + (1-f_Q)\right] + Q_{HA}\right\rangle} \quad (1)$$

DMD Fast Forward. Published on April 20, 2016 as DOI: 10.1124/dmd.116.069542
This article has not been copyedited and formatted. The final version may differ from this version.

$$\frac{v_L}{v_I+v_L}=\frac{E_L\left\langle Q_I\left[f_Q F_I+(1-f_Q)\right]+Q_{HA}\right\rangle}{f_Q Q_I(1-F_I)+E_L\left\langle Q_I\left[f_Q F_I+(1-f_Q)\right]+Q_{HA}\right\rangle} \quad (2)$$

The %contribution by the intestinal are 46 to 57% for the TM-PBPK and 9.3 to 17% for the SFM-PBPK, and the %contribution by the liver are 43 to 54% for the TM-PBPK and 83 to 91% for the SFM-PBPK (Table 7). These values differed due to the two methods for measuring F_I and F_L. The data shows that the SFM predicts a lesser contribution by the intestine for intestinal-liver removal of M when M in systemic circulation was presented to the intestine. The simulated $\frac{A^{MG}_{urine,4h,ID}}{A^{MG}_{bile,4h,ID}}$, $\frac{A^{MG}_{urine,4h,IV}}{A^{MG}_{bile,4h,IV}}$, and $\frac{A^{MG}_{urine,4h,ID}}{A^{MG}_{bile,4h,ID}}/\frac{A^{MG}_{urine,4h,IV}}{A^{MG}_{bile,4h,IV}}$ for the SFM-PBPK model were closer to the observations than those for the TM-PBPK (Table 8). These values were not changed dramatically when upon extrapolation of the data to infinity.

Mass balance solutions for TM-PBPK vs. SFM-PBPK. We also probed the mass-balance relations for TM vs. SFM. In this examination, several assumptions were made so that meaningful relations could be obtained easily: M is completely absorbed for the ID dose (F_{abs} = 1) but there is no enterohepatic recirculation for M secreted back to the lumen; M only forms MG and not other metabolites in the intestine and liver. These assumptions are quite reasonable in view of the fitted results (Tables 5 and 7). We further included renal excretion of M, with f_e to define the fraction of the IV dose of M excreted unchanged. The most important assumption was that MG in the systemic circulation does not enter the intestine or liver, but is renally excreted**.**

TM-PBPK. According to the TM-PBPK, the serial blood circuit delivering M and MG to the enterocyte (or whole intestine) region and the liver remains unchanged for both IV and ID dosing. The intestine exerts its strategic, anterior placement over the liver in its initial removal of

DMD Fast Forward. Published on April 20, 2016 as DOI: 10.1124/dmd.116.069542
This article has not been copyedited and formatted. The final version may differ from this version.

substrates before the species reach the liver. The extent of MG formation by both the intestine and liver is given by ($E_I + F_I E_H$). Thus the %contribution to MG formulation during first-pass by the intestinal and liver are $\frac{E_I}{E_I + F_I\ E_L}$ and $\frac{F_I\ E_L}{E_I + F_I\ E_L}$, respectively. These fractions, when multiplied by the appropriate organ available fractions for MG, $F\{mi\}_I$ and $F\{mi\}_L$ for the formed metabolite, yield the extents of formed MG entering the circulation $\left[\frac{E_I F\{mi\}_I}{E_I + F_I\ E_L} + \frac{F_I\ E_L\ F\{mi\}_L}{E_I + F_I\ E_L}\right]$. For the intestine and liver, the portions of the MG formed that are immediately excreted into the gut lumen and bile, respectively, are given by the extraction ratios, $E\{mi\}_I$ and $E\{mi\}_L$. For ID and IV doses of M ($Dose^M_{ID}$ and $Dose^M_{IV}$), the amounts of MG in urine and bile for TM are given by

$$A^{MG,TM}_{urine,ID} = E_I F\{mi\}_I Dose^M_{ID} + F_I\ E_L\ Dose^M_{ID} F\{mi\}_L + F_I\ F_L\ (1\text{-}f_e) Dose^M_{ID}\left[\frac{E_I F\{mi\}_I}{E_I + F_I\ E_L} + \frac{F_I\ E_L\ F\{mi\}_L}{E_I + F_I\ E_L}\right] \quad (3)$$

$$A^{MG,\,TM}_{bile,ID} = F_I\ E_L\ Dose^M_{ID} E\{mi\}_L + F_I\ F_L\ (1\text{-}f_e) Dose^M_{ID}\frac{F_I\ E_L\ E\{mi\}_L}{E_I + F_I\ E_L} \quad (4)$$

$$A^{MG,TM}_{urine,IV} = (1\text{-}f_e) Dose^M_{IV}\frac{\left(E_I F\{mi\}_I + F_I\ E_L\ F\{mi\}_L\right)}{E_I + F_I\ E_L} \quad (5)$$

$$A^{MG,TM}_{bile,IV} = (1\text{-}f_e) Dose^M_{IV}\frac{F_I\ E_L\ E\{mi\}_L}{E_I + F_I\ E_L} \quad (6)$$

The ratios of the amounts of MG in urine/bile for IV and ID dosing of M are identical

$$\frac{A^{MG,\,TM}_{urine,IV}}{A^{MG,\,TM}_{bile,IV}} = \frac{E_I F\{mi\}_I}{F_I\ E_L\ E\{mi\}_L} + \frac{F\{mi\}_L}{E\{mi\}_L} \quad (7)$$

DMD Fast Forward. Published on April 20, 2016 as DOI: 10.1124/dmd.116.069542
This article has not been copyedited and formatted. The final version may differ from this version.

$$\frac{A^{MG,\,TM}_{urine,ID}}{A^{MG,\,TM}_{bile,ID}} = \frac{E_I F\{mi\}_I}{F_I\ E_L\ E\{mi\}_L} + \frac{F\{mi\}_L}{E\{mi\}_L} = \frac{A^{MG,\,TM}_{urine,IV}}{A^{MG,\,TM}_{bile,IV}} \quad (8)$$

In like fashion, it may be shown that $\frac{A^{MG,TM}_{bile,ID}}{A^{MG,TM}_{bile,IV}} = \frac{A^{MG,TM}_{urine,\ ID}}{A^{MG,TM}_{urine,IV}}$ for TM-PBPK**.**

SFM-PBPK. According to the SFM-PBPK, MG is formed by the intestine and liver during the first pass effect, but mostly from the liver upon recirculation due to the segregated flow pattern to the enterocyte region (Cong et al., 2000). With the assumption that circulating levels of M cannot reach the enterocyte region for intestinal metabolism, the amounts of MG detected into urine (A^{MG}_{urine}) and bile (A^{MG}_{bile}) according to the SFM for ID and IV dosing of M are given by:

$$A^{MG,SFM}_{urine,ID} = E_I F\{mi\}_I Dose^M_{ID} + F_I\ Dose^M_{ID} E_L\ F\{mi\}_L + F_I\ F_L\ (1\text{-}f_e) Dose^M_{ID} F\{mi\}_L \quad (9)$$

$$A^{MG,\,SFM}_{bile,ID} = F_I\ E_L\ Dose^M_{ID} E\{mi\}_L + F_I\ F_L\ (1\text{-}f_e) Dose^M_{ID} E\{mi\}_L \quad (10)$$

$$A^{MG,SFM}_{urine,IV} = (1\text{-}f_e) Dose^M_{IV} F\{mi\}_L \quad (11)$$

$$A^{MG,SFM}_{bile,IV} = (1\text{-}f_e) Dose^M_{IV} E\{mi\}_L \quad (12)$$

The ratios of the amounts are

$$\frac{A^{MG,\,SFM}_{urine,\ ID}}{A^{MG,\,SFM}_{bile,ID}} = \frac{E_I F\{mi\}_I}{F_I E\{mi\}_L \left[E_L\ + F_L\ (1\text{-}f_e)\right]} + \frac{F\{mi\}_L}{E\{mi\}_L} \quad (13)$$

$$\frac{A^{MG,\,SFM}_{urine,IV}}{A^{MG,\,SFM}_{bile,IV}} = \frac{(1\text{-}f_e) Dose^M_{IV} F\{mi\}_L}{(1\text{-}f_e) Dose^M_{IV} E\{mi\}_L} = \frac{F\{mi\}_L}{E\{mi\}_L} \quad (14)$$

$\frac{A^{MG,\,SFM}_{urine,ID}}{A^{MG,\,SFM}_{bile,ID}}$ (Eq. 11) exceeds $\frac{A^{MG,\,SFM}_{urine,IV}}{A^{MG,\,SFM}_{bile,IV}}$ by $\frac{E_I F\{mi\}_I}{F_I E\{mi\}_L \left[E_L\ + F_L\ (1\text{-}f_e)\right]}$.

Similarly, the ratios of MG amounts in bile and urine after same doses of ID and IV of M are,

DMD Fast Forward. Published on April 20, 2016 as DOI: 10.1124/dmd.116.069542
This article has not been copyedited and formatted. The final version may differ from this version.

$$\frac{A^{MG,\,SFM}_{bile,ID}}{A^{MG,\,SFM}_{bile,IV}} = \frac{F_I\ E_L\ Dose^M_{ID}E\{mi\}_L\ +\ F_I\ F_L\ (1\text{-}f_e)Dose^M_{ID}E\{mi\}_L}{(1\text{-}f_e)Dose^M_{IV}E\{mi\}_L} = \frac{F_I\ E_L\ +\ F_I\ F_L\ (1\text{-}f_e)}{(1\text{-}f_e)} = \frac{F_I\ E_L}{(1\text{-}f_e)} + F_I\ F_L \qquad (15)$$

$$\frac{A^{MG,\,SFM}_{urine,ID}}{A^{MG,\,SFM}_{urine,IV}} = \frac{E_I F\{mi\}_I Dose^M_{ID}\ +\ F_I\ Dose^M_{ID}E_L\ F\{mi\}_L\ +\ F_I\ F_L\ (1\text{-}f_e)Dose^M_{ID}F\{MG\}_L}{(1\text{-}f_e)Dose^M_{IV}F\{mi\}_L} = \frac{E_I F\{mi\}_I}{(1\text{-}f_e)F\{mi\}_L} + \frac{F_I\ E_L}{(1\text{-}f_e)}\ +\ F_I\ F_L \qquad (16)$$

$\frac{A^{MG,\,SFM}_{urine,ID}}{A^{MG,\,SFM}_{urine,iv}}$ exceeds $\frac{A^{MG,\,SFM}_{bile,ID}}{A^{MG,\,SFM}_{bile,iv}}$ by $\frac{E_I F\{mi\}_I}{(1\text{-}f_e)F\{mi\}_L}$.

From the above analyses, differences are expected to exist between the TM-PBPK and SFM-PBPK. The identities: $\frac{A^{MG,TM}_{urine,ID}}{A^{MG,TM}_{urine,IV}} = \frac{A^{MG,TM}_{bile,ID}}{A^{MG,TM}_{bile,IV}}$ and $\frac{A^{MG,\,TM}_{urine,IV}}{A^{MG,\,TM}_{bile,IV}} = \frac{A^{MG,\,TM}_{urine,ID}}{A^{MG,\,TM}_{bile,ID}}$ exist for the TM, and these relations are in stark contrast to those shown for the SFM, where $\frac{A^{MG,\,SFM}_{urine,\,ID}}{A^{MG,\,SFM}_{urine,IV}} > \frac{A^{MG,\,SFM}_{bile,ID}}{A^{MG,\,SFM}_{bile,IV}}$ and $\frac{A^{MG,\,SFM}_{urine,ID}}{A^{MG,\,SFM}_{bile,ID}} > \frac{A^{MG,\,SFM}_{urine,IV}}{A^{MG,\,SFM}_{bile,IV}}$. For cases in which M from circulation would enter the intestine via $f_Q Q_I$, the true difference would fall in between unity (for TM) and the theoretical SFM-PBPK estimate from the above example, since MG is able to enter the liver from the circulation, and M is shunted away for metabolism by the intestine. These differences are exploited to discriminate between the SFM-PBPK and TM-PBPK. It is further interesting to note that, when there is complete absorption of M and absence of intestinal glucuronidation/secretion (F_I = 1 and E_I =0), $\frac{A^{MG,\,SFM}_{urine,ID}}{A^{MG,\,SFM}_{bile,ID}} = \frac{A^{MG,\,SFM}_{urine,IV}}{A^{MG,\,SFM}_{bile,IV}} = \frac{F\{MG\}_L}{E\{MG\}_L}$, and $\frac{A^{MG,\,SFM}_{bile,ID}}{A^{MG,\,SFM}_{bile,IV}} = \frac{A^{MG,\,SFM}_{urine,ID}}{A^{MG,\,SFM}_{urine,ID}} = \frac{E_L}{(1\text{-}f_e)} + F_L$.

DMD Fast Forward. Published on April 20, 2016 as DOI: 10.1124/dmd.116.069542
This article has not been copyedited and formatted. The final version may differ from this version.

DISCUSSION

With recognition that the intestine can significantly reduce the orally or intraduodenally absorbed dose during first-pass metabolism and that differential induction and inhibition patterns of the enzymes and transporters exists (for review, see Pang and Chow, 2012; Chow and Pang, 2013), much effort is extended to separate the contributions of the intestinal and liver in first-pass metabolism. The direct observations on intestinal metabolism could be deciphered for lorcainide metabolism in portacaval shunts in rodents (Gugler et al., 1975; Giacomini et al., 1980; Plänitz, et al., 1985) and midazolam oxidation in anhepatic patients after duodenal and intravenous administrations during transplant surgery (Paine et al., 1996). Others examined specific gene knockdown of Cyp3a and NADPH-cytochrome P450 reductase within the intestinal- versus hepatic-tissue to demonstrate directly the impact of the knockdown of intestinal vs. liver enzymes in first-pass metabolism *in vivo* (van Herwaarden et al., 2007; Zhang et al., 2007; 2009). The method of comparison of plasma or blood area under the curves of drug (AUCs) after oral, intraportal, and intravenous administration, supplemented by *in vitro* metabolic data, is commonly used to identify the presence of intestinal and extrahepatic vs. liver drug metabolism (Iwamoto and Klaassen, 1977; Iwamoto et al., 1982; Cassidy and Houston, 1984, Mistry and Houston, 1987; Liu et al., 2010). Judging merely from the AUC of the blood concentration of the MG or formed metabolite, AUC^{MG}, it becomes difficult to tease out each of the individual contributions of the intestine and liver since multiple tissues are involved in the formation and sequential metabolism of the metabolite (Sun and Pang, 2010). The situation becomes more complex for metabolite kinetics when the metabolite formed undergoes sequential elimination (by metabolism or excretion) (Pang and Gillette, 1979), when a permeability barrier exists (deLannoy and Pang 1986), and

DMD Fast Forward. Published on April 20, 2016 as DOI: 10.1124/dmd.116.069542
This article has not been copyedited and formatted. The final version may differ from this version.

when the intestine with segregated flow is involved for metabolite formation (Cong et al., 2000). The metabolism of M to MG by the intestine and liver and the immediate excretion of MG in the formation organs exemplify this situation.

The inadequacy of the compartmental model is shown readily. The compartmental approach (Fig.1) overpredicted MG excretion into bile for IV but underpredicted for ID dosing of M and overpredicted the excretion of MG in urine for IV, while underpredicting MG excretion for ID dosing. The CL was 8.8 $mL \cdot min^{-1}$ (Table 4), slightly overpredicting the observed CL_{tot} (6.57 $mL \cdot min^{-1}$); a higher F_{abs} of about 0.95 (Table 4) vs. that observed was obtained. Although the comparison of k_m/k_{10} yielded the extent of MG formation (67.5%), other important parameters are unobtainable (compare Table 4 to Tables 5 and 7).

In contrast, we obtain much more insight on M and MG handling with TM- and SFM-PBPK modeling. The final model consists of uptake, transport, and metabolic pathways of M and MG (Table 5), when the liver ($CL_{in,L}^{MG}$ as 1 $mL \cdot min^{-1}$) and intestinal ($CL_{in,I}^{MG}$ as 0 $mL \cdot min^{-1}$) influx clearances for MG were assigned (Fig. 2), and sequential removal of MG is via secretion, in contrast to other metabolites that may undergo further metabolism (Pang and Gillette, 1979). We had tested other PBPK models ($CL_{in,L}^{MG} = 0$ and $CL_{in,I}^{MG} > 0$), but the fit did not improve. The final model revealed information on the effective partitioning ratio into tissue (0.14 and 0.53 for intestine and 1.4 and 2.5 for liver based on TM-PBPK or SFM-PBPK model), estimates of h_{mi} and g_{mi}, the fractions of hepatic and total body clearance of M forming MG, respectively, with full accounting of the immediate excretion of the nascently-formed MG, as $F\{mi\}_I$ and $F\{mi\}_L$ (Table 7) Moreover, the estimates of F_I and F_L that dissect the contribution of the intestine and liver first-pass removal were provided. We emphasize that there are differences in intestinal metabolism

DMD Fast Forward. Published on April 20, 2016 as DOI: 10.1124/dmd.116.069542
This article has not been copyedited and formatted. The final version may differ from this version.

when M is entering the intestine from the circulation, and the SFM predicted a smaller intestinal contribution than the TM that during the recirculation of M (Table 7).

In pursuit of whether the SFM is superior over the TM to describe intestinal metabolism of morphine *in vivo*, we nested these intestinal models into the PBPK model for data fitting (Fig. 2). When both the intestine and liver are involved in formation of the metabolite, we illustrate that the metabolic data is best utilized to provide discrimination between the SFM-PBPK vs. TM-PBPK. Therefore, we examined the metabolism of M and excretion of MG. M enters cells freely by passive diffusion whereas the formed metabolite, MG, is poorly permeable across the intestine and liver basolateral membranes (Doherty et al., 2006; van de Wetering et al., 2007). MG formed in intestine and liver is effluxed out by Mrp3 or excreted by Mrp2 into the lumen or bile, respectively. The MG in bile originates mostly from M metabolism in the liver while some from MG formed from intestine and entered the liver, and is excreted into bile, whereas MG in urine originates from the intestine and liver. Thus, after taking some simple assumptions, differences are expected between the SFM-PBPK and TM-PBPK prediction based on our simple mass balance solutions on the ratio, $A_{urine}^{MG} / A_{bile}^{MG}$ after ID and IV dosing of M. The $A_{urine}^{MG,TM} / A_{bile}^{MG,TM}$ ratio according to the TM remains unchanged for both ID and IV dosing (Eq. 8) since, according to this model, the intestine exerts itself as the anterior organ within the intestine-liver unit, regardless of whether morphine is entering via the ID route or from the systemic circulation. With the extreme assumption that M in circulation is completely shunted away from the intestine and MG does not cross membranes into the intestine or liver, $A_{urine}^{MG,SFM} / A_{bile}^{MG,SFM}$ for SFM after ID dosing of M would exceed that for IV (Eq. 16). However, there is some delivery of M to the enterocyte region (namely, f_Q is not zero, but $f_Q \sim 0.1$) and $CL_{in,L}^{MG} = 1$ mL·min^{-1}. Clearly, the predictions for the SFM would fall between

DMD Fast Forward. Published on April 20, 2016 as DOI: 10.1124/dmd.116.069542
This article has not been copyedited and formatted. The final version may differ from this version.

this extreme condition for SFM and that for the TM. Indeed, we observed: $\frac{A^{MG}_{urine,ID}}{A^{MG}_{bile,ID}}(0.541) > \frac{A^{MG}_{urine,IV}}{A^{MG}_{bile,IV}}$ (0.212), and the ratio for $A^{MG}_{urine} / A^{MG}_{bile}$ after ID dosing of M being 2.55*x* that of IV dosing (Table 3). These observations agree well with the prediction of the SFM ratio, being greater than unity (Eq. 16), whereas that for TM (Eq. 8), the ratio is unity (Table 8). Moreover, the superior fit to the SFM model (Table 6 and Figs. 5 and 6), and the simulated patterns for M and MG correlated better with the observed data than TM (Figs. 4, 5 and 6) suggesting that SFM-PBPK describes first-pass removal of M and MG in rats *in vivo* much better than the TM-PBPK. With these observations, we may conclude that systemically delivered morphine is partially shunted away from reaching the enterocyte region containing the Ugt2b1 for glucuronidation.

The question that remains is why the urgency to identify the proper intestine model in PBPK modeling. Recent examination of intestinal flow models has emphasized that the type of intestinal flow model chosen is important: TM, Q_{Gut} model (Yang et al., 2007) or SFM, in which the fractional flow to enterocyte region (f_Q) is 1, 0.484, and 0.1-0.3, respectively (Pang and Chow, 2012). For most substrates, the fitted f_Q is < 0.2 (Pang and Chow, 2012; Chow and Pang, 2013), and is 0.10 for this study (Table 5). Since the %contribution of intestine during recirculation of M is dependent on f_Q (see equations shown as footnotes to Table 7), and we expect the ranking of SFM < Q_{Gut} model < TM to stand, whereas the opposite exists for the %contribution of liver: SFM > Q_{Gut} model > TM (Pang and Chow, 2012). These interpretations could affect the translation of *in vitro* microsomal activity to the metabolic intrinsic clearance, $CL_{int,met}$, *in vivo*. The intestinal flow model chosen to represent the enterocyte flow may also influence values of F_I and E_I. The data of Mistry and Houston (1987) revealed a 240-fold microsomal activity ratio

DMD Fast Forward. Published on April 20, 2016 as DOI: 10.1124/dmd.116.069542
This article has not been copyedited and formatted. The final version may differ from this version.

($CL_{int,met,L}/CL_{int,met,I}$) *in vitro*, and yet *in vivo* E_I and E_L values of 0.33 and 0.47, respectively, correlated to only a 37-fold intrinsic clearance ratio (calculated $CL_{int,met,L}/CL_{int,met,I}$) *in vivo* for morphine glucuronidation in the rat. Therefore, the flow pattern to the enterocyte region of the intestine may play a role to alter *in vitro-in vivo* extrapolation.

Data from the present study supports the view that the SFM-PBPK is superior over other intestinal flow models (Q_{Gut} or TM, for example). There has been some movement in the field to accommodate a reduced or partial intestinal flow to the enterocyte region. The emergence of the Q_{Gut} model (Yang et al., 2007) and the ADAM model from Simcyp® (Darwich et al., 2010) favors this concept of partial flow. Other models that further encompass heterogeneity in transporters and enzymes have been adopted to explain the lesser intestinal metabolism observed for drugs given systemically vs. orally (Tam et al., 2003; Liu et al., 2006; Gertz et al., 2010; Bruyère et al., 2010) as well as the impact of enterohepatic circulation of glucuronide conjugates (Wu et al., 2011). Undoubtedly, the present PBPK investigation strongly supports the SFM for intestinal modeling. More importantly, the modeling approach provided essential information on the interpretation of metabolite kinetics.

DMD Fast Forward. Published on April 20, 2016 as DOI: 10.1124/dmd.116.069542
This article has not been copyedited and formatted. The final version may differ from this version.

ACKNOWLEDGEMENT S

We thank Dr. Carolyn Cummins of the Leslie Dan Faculty of Pharmacy, University of Toronto for use of her LCMS equipment.

AUTHORSHIP CONTRIBUTIONS

Participated in research design: J Fan, S Chen, and KS Pang

Conducted experiments: S Chen, J Fan, H Sun

Performed data analysis: QJ Yang, J Fan, S Chen, L Liu, H Sun, and KS Pang

Wrote or contributed to the writing of the manuscript: QJ Yang, J Fan, S Chen, and KS Pang

REFERENCE

Böerner U (1975) The metabolism of morphine and heroin in man. *Drug Metab Rev* **4:**39-73.

Boxenbaum HG, Riegelman S, and Elashoff RM (1974) Statistical estimations in pharmacokinetics. *J Pharmacokinet Biopharm* **2**:123-148.

Bruyère A, Declèves X, Bouzom F, Ball K, Marques C, Treton X, Pocard M, Valleur P, Bouhnik Y, Panis Y, Scherrmann JM, and Mouly S (2010) Effect of variations in the amounts of P-glycoprotein (ABCB1), BCRP (ABCG2) and CYP3A4 along the human small intestine on PBPK models for predicting intestinal first pass. *Mol Pharm* **7:**1596–1607.

Cassidy MK and Houston JB (1984) In vivo capacity of hepatic and extrahepatic enzymes to conjugate phenol. *Drug Metab Dispos* **12**:619-624.

Chow EC and Pang KS (2013) Why we need proper PBPK models to examine intestine and liver oral drug absorption. *Curr Drug Metab* **14**:57-79. Review

Cong D, Doherty M, and Pang KS (2000) A new physiologically based, segregated-flow model to explain route-dependent intestinal metabolism. *Drug Metab Dispos* **28:**224-235.

Corley RA, Bartels MJ, Carney EW, Weitz KK, Soelberg JJ, Gies RA, and Thrall KD (2005) Development of a physiologically based pharmacokinetic model for ethylene glycol and its metabolite, glycolic acid, in rats and humans. *Toxicol Sci* **85:** 476-490.

Dahlström BE and Paalzow LK (1978) Pharmacokinetic interpretation of the enterohepatic recirculation and first-pass elimination of morphine in the rat. *J Pharmacokinet Biopharm* **6:**505-519.

Darwich AS, Neuhoff S, Jamei M, and Rostami-Hodjegan A (2010) Interplay of metabolism and transport in determining oral drug absorption and gut wall metabolism: a simulation assessment using the "advanced dissolution, absorption, metabolism (ADAM)" model. *Curr Drug Metab* **11**:716-29.

Davies B and Morris T (1993) Physiological parameters in laboratory animals and humans. *Pharm Res* **10**:1093-1095.

deLannoy IA and Pang KS (1986) Presence of a diffusional barrier on metabolite kinetics: enalaprilat as a generated versus preformed metabolite. *Drug Metab Dispos* **14**:513-520.

deLannoy IA and Pang KS (1993) Combined recirculation of the rat liver and kidney: studies with enalapril and enalaprilat. *J Pharmacokinet Biopharm* **21**:423-456.

De Vries PAM, Navis G, de Boer E, de Jong PE, and de Zeeuw D (1997) A method for accurate measurement of GFR in conscious spontaneously voiding rats. *Kidney Int* **52**:244-247.

Doherty MM and Pang KS (2000) Route-dependent metabolism of morphine in the vascularly perfused rat small intestine preparation. *Pharm Res* **17:**291-298.

Doherty MM, Poon K, Tsang C, and Pang KS (2006) Transport is not rate-limiting in morphine glucuronidation in the single-pass perfused rat liver preparation. *J Pharmacol Exp Ther* **317**(2):890-900.

Everett NB, Simmons B, and Lasher EP (1956) Distribution of blood (Fe^{59}) and plasma (I^{113}) volumes of rats determined by liquid nitrogen freezing. *Circ Res* **4**:419-424.

Fan J, Chen S, Chow EC, and Pang KS (2010) PBPK modeling of intestinal and liver enzymes and transporters in drug absorption and sequential metabolism. *Curr Drug Metab* **11**:743-61. Review.

Gao G and Law FC (2009) Physiologically based pharmacokinetics of matrine in the rat after oral administration of pure chemical and ACAPHA. *Drug Metab Dispos* **37**:884-891.

Gertz M, Harrison A, Houston JB, and Galetin A (2010) Prediction of human intestinal first-pass metabolism of 25 CYP3A substrates from in vitro clearance and permeability data. *Drug Metab Dispos* **38**:1147–1158.

Giacomini KM, Nakeeb SM, and Levy G (1980) Pharmacokinetic studies of propoxyphene I: Effect of portacaval shunt on systemic availability in dogs. *J Pharm Sci* **69**:786-789.

Gugler R, Lain P, and Azarnoff DL (1975) Effect of portacaval shunt on the disposition of drugs with and without first-pass effect. *J Pharmacol Exp Ther* **195**:416-423.

Hirayama H, Morgado J, Gasinska I, and Pang KS (1990) Estimations of intestinal and liver first-pass metabolism in vivo. Studies on gentisamide conjugation in the rat. *Drug Metab Dispos* **18**:580-587.

Horton TL and Pollack GM (1991) Enterohepatic recirculation and renal metabolism of morphine in the rat. *J Pharm Sci* **80:**1147-1152.

Iwamoto K and Klaassen CD (1977) First-pass effect of morphine in rats. *J Pharmacol Exp Ther* **200:**236-244.

Iwamoto K, Takei M, and Watanabe J (1982) Gastrointestinal and hepatic first-pass metabolism of aspirin in rats. *J Pharm Pharmacol* **34**:176-180.

Letrent SP, Polli JW, Humphreys JE, Pollack GM, Brouwer KR, and Brouwer KL (1999) P-glycoprotein-mediated transport of morphine in brain capillary endothelial cells. *Biochem Pharmacol* **58:**951-957.

Liu S, Tam D, Chen X, and Pang KS (2006) P-Glycoprotein and an unstirred water layer barring digoxin absorption in the vascularly perfused rat small intestine preparation: induction studies with pregnenolone-16α-carbonitrile. *Drug Metab Dispos* **34:**1468-1479.

Liu YT, Hao HP, Xie HG, Lai L, Wang Q, Liu CX, and Wang GJ (2010) Extensive intestinal first-pass elimination and predominant hepatic distribution of berberine explain its low plasma levels in rats. *Drug Metab Dispos* **38**:1779-1784.

Lown KS, Thummel KE, Benedict PE, Shen DD, Turgeon DK, Berent S, and Watkins PB (1995) The erythromycin breath test predicts the clearance of midazolam. *Clin Pharmacol Ther* **57:**16-24.

Mistry M and Houston JB (1987) Glucuronidation in vitro and in vivo. Comparison of intestinal and hepatic conjugation of morphine, naloxone and buprenorphine. *Drug Metab Dispos* **15**(5):710-717.

Paine MF, Shen DD, Kunze KL, Perkins JD, Marsh CL, McVicar JP, Barr DM, Gilles BS, and Thummel KE (1996) First-pass metabolism of midazolam by the human intestine. *Clin Pharmacol Ther* **60:**14–24.

Pang KS (2009) Safety testing of metabolites: Expectations and outcomes. *Chem Biol Interact* **179**:45-59. Review.

Pang KS (2003) Modeling of intestinal drug absorption: roles of transporters and metabolic enzymes (for the Gillette Review Series). *Drug Metab Dispos* **31:**1507-1519.

Pang KS and Chow EC (2012) Commentary: Theoretical predictions of flow effects on intestinal and systemic availability in physiologically based intestine models: the traditional model, segregated flow model, and Q_{Gut} model. *Drug Metab Dispos* **40**:1869-1877.

Pang KS and Gillette JR (1979) Sequential first-pass elimination of a metabolite derived from a precursor. *J Pharmacokinet Biopharm* **7**:275-290.

Pang KS and Kwan KC (1983) A commentary: methods and assumptions in the kinetic estimation of metabolite formation. *Drug Metab Dispos* **11:**79-84.

Pang KS, Maeng HJ, and Fan J (2009) Interplay of transporters and enzymes in drug and metabolite processing. Mol Pharm **6**:1734-1755.

Pang KS, Morris ME, and Sun H (2008) Formed and preformed metabolite: Facts and comparisons. *J Pharm Pharmacol* **60**:1247-1275.

Pang KS, Cherry WF, and Ulm EH (1985) Disposition of enalapril in the perfused rat intestine-liver preparation: absorption, metabolism and first-pass effect. *J Pharmacol Exp Ther* **233**:788-795.

Peters SA (2008) Identification of intestinal loss of a drug through physiologically based pharmacokinetic simulation of plasma concentration-time profiles. *Clin Pharmacokinet* **47**(4): 245-259.

Plänitz V, Grönniger J, and Jähnchen E (1985) Prehepatic and hepatic first-pass metabolism of lorcainide in rats. *Arzneimittelforschung* **35**:923-926.

Projean D, Morin PE, Tu TM, and Ducharme J (2003) Identification of CYP3A4 and CYP2C8 as the major cytochrome P450 s responsible for morphine N-demethylation in human liver microsomes. *Xenobiotica* **33:**841-854.

Qi X, Evans AM, Wang J, Miners JO, Upton RN, and Milne RW (2010) Short communication. Inhibition of morphine metabolism by ketamine. *Drug Metab Dispos* **38**:728–731.

Rane A, Gawronska-Szklarz B, Svensson JO (1985) Natural (-)- and unnatural (-)-enantiomers of morphine: comparative metabolism and effect of morphine and phenobarbital treatment. *J Pharmacol Exp Ther* **234**:761–765.

Rodgers T and Rowland M (2006) Physiologically based pharmacokinetic modeling 2: predicting the tissue distribution of acids, very weak bases, neutrals and zwitterions. *J Pharm Sci* **95**:1238-1257.

Rodgers T and Rowland M (2007) Mechanistic approaches to volume of distribution predictions: understanding the processes. *Pharm Res* **24**:918-933.

Shanahan KM, Evans AM, and Nation RL (1997) Disposition of morphine in the rat isolated perfused kidney: concentration ranging studies**.** *J Pharmacol Exp Ther* **282**:1518-1525.

Sun H and Pang KS (2010) Physiological modeling to understand the impact of enzymes and transporters on drug and metabolite data and bioavailability estimates. *Pharm Res* **27**:1237-1254.

Sun H, Liu L, and Pang KS (2006) Increased estrogen sulfation of estradiol 17β-D-glucuronide in metastatic tumor rat livers. *J Pharmacol Exp Ther* **319**:818-831.

Sun GH, Zeng YY, and Pang KS (2010) Interplay of phase II enzymes and transporters in futile cycling: influence of multidrug resistance-associated protein 2-mediated excretion of estradiol 17β-D-glucuronide and its 3-sulfate metabolite on net sulfation in perfused TR(-) and Wistar rat liver preparations. *Drug Metab Dispos* **38**:769-780.

Tam D, Tirona RG, and Pang KS (2003) Segmental intestinal transporters and metabolic enzymes on intestinal drug absorption. *Drug Metab Dispos* **31**:373-383.

Van Crugten JT, Sallustio BC, Nation RL, and Somogyi AA (1991) Renal tubular transport of morphine, morphine-6-glucuronide, and morphine-3-glucuronide in the isolated perfused rat kidney. *Drug Metab Dispos* **19**:1087-1092.

van de Wetering K, Zelcer N, Kuil A, Feddema W, Hillebrand M, Vlaming ML, Schinkel AH, Beijnen JH and Borst P (2007) Multidrug resistance proteins 2 and 3 provide alternative routes for hepatic excretion of morphine-glucuronides. *Mol Pharmacol* **72:**387-394.

van Herwaarden AE, Wagenaar E, van der Kruijssen CM, van Waterschoot RA, Smit JW, Song JY, van der Valk MA, van Tellingen O, van der Hoorn JW, Rosing H, Beijnen JH, and Schinkel AH (2007) Knockout of cytochrome P450 3A yields new mouse models for understanding xenobiotic metabolism. *J Clin Invest* **117**:3583-3592.

Wandel C, Kim R, Wood M and Wood A (2002) Interaction of morphine, fentanyl, sufentanil, alfentanil, and loperamide with the efflux drug transporter P-glycoprotein. *Anesthesiology* **96:** 913-920.

Wu B (2011) Use of physiologically based pharmacokinetic models to evaluate the impact of intestinal glucuronide hydrolysis on the pharmacokinetics of aglycone. *J Pharm Sci* **101**:1281-1301.

Yang J, Jamei M, Yeo KR, Tucker GT and Rostami-Hodjegan A (2007) Prediction of intestinal first-pass drug metabolism. *Curr Drug Metab* **8:**676-684.

Zhang QY, Fang C, Zhang J, Dunbar D, Kaminsky L, and Ding X (2009) An intestinal epithelium-specific cytochrome P450 (P450) reductase-knockout mouse model: direct evidence for a role of intestinal P450s in first-pass clearance of oral nifedipine. *Drug Metab Dispos* **37**:651–657.

Zhang QY, Kaminsky L, Dunbar D, Zhang J, and Ding X (2007) Role of small intestinal cytochromes P450 in the bioavailability of oral nifedipine. *Drug Metab Dispos* **35**:1617–1623.

DMD Fast Forward. Published on April 20, 2016 as DOI: 10.1124/dmd.116.069542
This article has not been copyedited and formatted. The final version may differ from this version.

APPENDIX A: Equations for compartmental modeling

Rate of change of M in gut lumen for intraduodenal (ID) dosing

$$\frac{dA_G}{dt} = -k_a A_G \text{ ; where } A_G(0) = F_{abs} \cdot dose_{ID} \quad (1)$$

Rates of change of M in central compartment

$$\frac{dC_1}{dt} = \frac{\left(-(k_{10}+k_{12})C_1V_1 + k_aA_G + k_{21}C_2V_2\right)}{V_1} \quad \text{for ID dosing} \quad (2)$$

$$\frac{dC_1}{dt} = \frac{\left(-(k_{10}+k_{12})C_1V_1 + k_{21}C_2V_2\right)}{V_1} \quad \text{for IV dosing} \quad (2A)$$

Rates of change of M in peripheral compartment

$$\frac{dC_2}{dt} = \frac{\left(-k_{21}C_2V_2 + k_{12}C_1V_1\right)}{V_2} \quad (3)$$

Rate of change of MG or formed metabolite, denoted as {mi}

$$\frac{dC\{mi\}}{dt} = \frac{k_mC_1V_1 - k\{mi\}C\{mi\}\ V\{mi\}}{V\{mi\}} \quad (4)$$

Rates of biliary excretion of M and MG

$$\frac{dA_{bile}}{dt} = k_{bile}C_1V_1 \quad (5)$$

$$\frac{dA\{mi\}_{bile}}{dt} = k\{mi\}_{bile}C\{mi\}V\{mi\} \quad (6)$$

Rates of renal excretion of M and MG

$$\frac{dA_{renal}}{dt} = k_{renal}C_1V_1 \quad (7)$$

DMD Fast Forward. Published on April 20, 2016 as DOI: 10.1124/dmd.116.069542
This article has not been copyedited and formatted. The final version may differ from this version.

$$\frac{dA\{mi\}_{renal}}{dt} = k\{mi\}_{renal} C\{mi\} V\{mi\} \quad (8)$$

APPENDIX B: Equations for PBPK modeling

Several assumptions were made: deglucuronidation of M was absent and reabsorption of MG was absent (Doherty and Pang, 2000). Once formed in the intestine or tissue, MG is effluxed out apically by Mrp2 or basolaterally by Mrp3 (van de Wetering et al., 2007) with efflux clearances, $CL_{ef,I}^{MG}$ and $CL_{ef,L}^{MG}$, respectively, for the intestine and liver. MG permeates through liver basolateral membrane with rate of 1 mL·min^{-1} of liver (Doherty et al., 2006) but not through the intestine membrane for secretion (Doherty and Pang, 2000).

Rate of change of M and MG in blood compartment

$$V_B \frac{dM_B}{dt} = Q_{RP}\frac{M_{RP}}{K_{RP}} + Q_{PP}\frac{M_{PP}}{K_{PP}} + Q_{AD}\frac{M_{AD}}{K_{AD}} + (Q_I + Q_{HA})M_{LB} - (Q_I + Q_{HA} + Q_{RP} + Q_{PP} + Q_{AD})M_B - f_B M_B CL_R^M \quad (9)$$

$$V_B \frac{dMG_B}{dt} = (Q_I + Q_{HA})(MG_{LB} - MG_B) - f_B MG_B CL_R^{MG} \quad (10)$$

Rate of change of M in rapidly perfused tissue

$$V_{RP} \frac{dM_{RP}}{dt} = Q_{RP}M_B - Q_{RP}\frac{M_{RP}}{K_{RP}} \quad (11)$$

Rate of change of M in poorly perfused tissue

$$V_{PP} \frac{dM_{PP}}{dt} = Q_{PP}M_B - Q_{PP}\frac{M_{PP}}{K_{PP}} \quad (12)$$

Rate of change of M in adipose tissue

$$V_{AD} \frac{dM_{AD}}{dt} = Q_{AD}M_B - Q_{AD}\frac{M_{AD}}{K_{AD}} \quad (13)$$

For intestine and liver for the TM,

Rate of change of M and MG in intestine, I (TM)

$$V_I \frac{dM_I}{dt} = f_B^M M_{IB} CL_{in,I}^M - f_I^M M_I (CL_{int,met,I}^{M\rightarrow MG} + CL_{int,sec,I}^M + CL_{ef,I}^M) + k_a A_{lumen}^M \quad (14)$$

$$V_I \frac{dMG_I}{dt} = f_i^M M_I CL_{int,met,I}^{M\rightarrow MG} - f_i^{MG} MG_I \left(CL_{int,sec,I}^{MG} + CL_{ef,I}^{MG}\right) \quad (15)$$

DMD Fast Forward. Published on April 20, 2016 as DOI: 10.1124/dmd.116.069542
This article has not been copyedited and formatted. The final version may differ from this version.

Rate of change of M and MG in intestine blood, IB (TM)

$$V_{IB}\frac{dM_{IB}}{dt} = Q_I(M_B - M_{IB}) - f_B^M M_{IB} CL_{In,I}^M + f_I^M M_I CL_{ef,I}^M \quad (16)$$

$$V_{IB}\frac{dMG_{IB}}{dt} = Q_I(MG_B - MG_{IB}) + f_I^{MG} MG_I CL_{ef,I}^{MG} \quad (17)$$

Rate of change of M and MG in liver, L (TM)

$$V_L\frac{dM_L}{dt} = f_B^M M_{LB} CL_{in,L}^M - f_L^M M_L (CL_{int,met,L}^{M\to MG} + CL_{int,met,L}^{M\to Others} + CL_{int,sec,L}^M + CL_{ef,L}^M) \quad (18)$$

$$V_L\frac{dMG_L}{dt} = f_L^M M_L CL_{int,met,L}^{M\to MG} - f_L^{MG} MG_L \left(CL_{int,sec,L}^{MG} + CL_{ef,L}^{MG}\right) + f_B^{MG} MG_{LB} CL_{in,L}^{MG} \quad (19)$$

Rate of change of M and MG in liver blood, LB (TM)

$$V_{LB}\frac{dM_{LB}}{dt} = Q_{HA}M_B + Q_I M_{IB} - (Q_{HA} + Q_I)M_{LB} + f_L^M M_L CL_{ef,L}^M - f_B^M M_{LB} CL_{in,L}^M \quad (20)$$

$$V_{LB}\frac{dMG_{LB}}{dt} = Q_{HA}MG_B + Q_I MG_{IB} - (Q_{HA} + Q_I)MG_{LB} + f_L^{MG} MG_L CL_{ef,L}^{MG} - f_B^{MG} MG_{LB} CL_{in,L}^{MG} \quad (21)$$

For intestine and liver for the SFM,

Rate of change of M and MG in enterocyte, en (SFM)

$$V_{en}\frac{dM_{en}}{dt} = f_B^M M_{enb} CL_{in,I}^M - f_I^M M_{en} (CL_{int,met,I}^{M\to MG} + CL_{int,sec,I}^M + CL_{ef,I}^M) + k_a A_{lumen}^M \quad (22)$$

$$V_{en}\frac{dMG_{en}}{dt} = f_I^M M_{en} CL_{int,met,I}^{M\to MG} - f_I^{MG} MG_{en} (CL_{ef,I}^{MG} + CL_{int,sec,I}^{MG}) \quad (23)$$

Rate of change of M and MG in enterocyte blood, enB (SFM)

$$V_{enB}\frac{dM_{enB}}{dt} = f_Q Q_I (M_B - M_{enB}) + f_I^M M_{en} CL_{ef,I}^M - f_B^M M_{enB} CL_{In,I}^M \quad (24)$$

$$V_{enB}\frac{dMG_{enB}}{dt} = f_Q Q_I (MG_B - MG_{enB}) + f_I^{MG} MG_{en} CL_{ef,I}^{MG} \quad (25)$$

Rate of change of M and MG in serosa, s (SFM)

DMD Fast Forward. Published on April 20, 2016 as DOI: 10.1124/dmd.116.069542
This article has not been copyedited and formatted. The final version may differ from this version.

$$V_s \frac{dM_s}{dt} = f_B^M M_{sB} CL_{in,I}^M - f_I^M M_s CL_{ef,I}^M \quad (26)$$

$$V_s \frac{dMG_s}{dt} = 0$$

Rate of change of M and MG in serosal blood, sB (SFM)

$$V_{sB} \frac{dM_{sB}}{dt} = (1-f_Q)Q_I(M_B - M_{sB}) + f_I^M M_s CL_{ef,I}^M - f_B^M M_{sB} CL_{In,I}^M \quad (27)$$

$$V_{sB} \frac{dMG_{sB}}{dt} = 0$$

Rate of change of M and MG in liver blood, LB (SFM)

$$V_{LB} \frac{dM_{LB}}{dt} = Q_{HA} M_B + f_Q Q_I M_{enB} + (1-f_Q)Q_I M_{sB} - (Q_{HA} + Q_I)M_{LB} + f_L^M M_L CL_{ef,L}^M - f_B^M M_{LB} CL_{in,L}^M \quad (28)$$

$$V_{LB} \frac{dMG_{LB}}{dt} = Q_{HA} MG_B + f_Q Q_I MG_{enB} + (1-f_Q)Q_I MG_{sB} - (Q_{HA} + Q_I)MG_{LB} + f_L^{MG} MG_L CL_{ef,L}^{MG} - f_B^{MG} MG_{LB} CL_{in,L}^{MG} \quad (29)$$

Rate of change of M and MG in liver, L (SFM): same equations (equations 20 and 21) as for TM

Rate of change of M and MG in gut lumen

$$\frac{dA_{lumen}^M}{dt} = -k_a A_{lumen}^M + f_I^M M_I CL_{int,sec,I} \quad (TM)$$
$$\text{or } -k_a A_{lumen}^M + f_I^M M_{en} CL_{int,sec,I} \quad (SFM) \quad (30)$$

$$\frac{dA_{lumen}^{MG}}{dt} = f_I^{MG} MG_I CL_{int,sec,I}^{MG} \quad (\text{for TM})$$
$$\text{or } f_I^{MG} MG_{en} CL_{int,sec,I}^{MG} \quad (\text{for SFM}) \quad (31)$$

Rate of change of M and MG in bile for both TM and SFM

$$\frac{dA_{bile}^M}{dt} = f_L^M M_L CL_{int,sec,L} \quad (32)$$

$$\frac{dA_{bile}^{MG}}{dt} = f_L^{MG} MG_L CL_{int,sec,L}^{MG} \quad (33)$$

Rate of change of M and MG in urine for both TM and SFM

DMD Fast Forward. Published on April 20, 2016 as DOI: 10.1124/dmd.116.069542
This article has not been copyedited and formatted. The final version may differ from this version.

$$\frac{dA_{urine}^{M}}{dt} = f_B^M M_B CL_R^M \quad (34)$$

$$\frac{dA_{urine}^{MG}}{dt} = f_B^{MG} MG_B CL_R^{MG} \quad (35)$$

FOOTNOTES

QJY and JF are Co-first authors.

This work was supported by the Canadian Institutes of Health Research (KSP) and the Ontario Graduate Scholarship Program (QJY).

DMD Fast Forward. Published on April 20, 2016 as DOI: 10.1124/dmd.116.069542
This article has not been copyedited and formatted. The final version may differ from this version.

LEGENDS

Figure 1 **The two-compartment model scheme for describing the pharmacokinetics of morphine (M) and morphine 3β-glucuronide (MG (or {mi}) (as one compartment);** concentrations and amounts have been normalized to dose. k_{renal}, k_{bile}, $k_{m,others}$ and k_m are the first-order rate constants describing M elimination via excretion by the kidney and liver, and metabolism to MG formation or other metabolites; $k\{mi\}_{renal}$, $k\{mi\}_{bile}$ denote the first-order excretion rate constants of MG (or {mi}) by the kidney and liver, respectively.

Figure 2 TM-PBPK (A) and SFM-PBPK (B) models for describing the pharmacokinetics of morphine (M) and morphine 3β-glucuronide (MG). MG exhibits poor entry into tissues (including the intestine and liver) and MG is formed in the intestine and liver. Intestinally formed MG, entering the liver with influx clearance ($CL_{in,L}^{MG}$) of 1 $mL \cdot min^{-1}$ (according to Doherty et al. 2006), and MG formed in the liver are excreted into bile. See text for details for the definition of terms.

Figure 3 Observed blood concentration-time profiles of morphine (M) and morphine 3-glucuronide (MG) as well as the cumulative amounts of M and MG in bile and urine following IV(A) and ID dosing (B) of M (IV, solid circles, n=4; ID, open circles, n=3; M and MG are denoted as red and blue symbols). The fits of the compartmental model (lines) to blood concentrations of M and MG, and the cumulative amounts of M and MG in bile and urine following intravenous and ID administration of M are shown. Data are mean±S.D.

Figure 4 Observed blood concentration-time profiles of morphine (M) and morphine 3-glucuronide (MG) as well as the cumulative amounts of M and MG in bile and urine following IV (A) or ID (B) administration of M (IV, solid circles, n=4; ID, open circles, n=3; M: red and MG: blue). Fitting was performed according to the TM or SFM models nested in PBPK models (TM-PBPK or SFM-PBPK). The fit of the model to blood concentrations of M and MG, and cumulative amounts of M and MG in bile and urine following intravenous and ID administration of M (SFM: solid line; TM: dashed line). Data are mean±S.D and same as those in Figure 3. Note the improved correlation between predictions and observations for M and MG for the SFM and the less optimal fit of MG with the TM.

Figure 5. Plots of observations versus predictions for morphine (M, red) and morphine 3-glucuronide (MG, blue) in blood, bile and urine following IV (solid symbols) or ID (open symbols) administration using TM-PBPK. The black line denotes the line of identity.

Figure 6. Plots of observations versus predictions for morphine (M, red) and morphine 3-glucuronide (MG, blue) in blood, bile and urine following IV (solid symbols) or ID (open symbols) administration using SFM-PBPK. The black line denotes the line of

identity. Note that the SFM-PBPK showed here shows a superior correlation between predictions and observations compared to the TM-PBPK (Fig. 5).

DMD Fast Forward. Published on April 20, 2016 as DOI: 10.1124/dmd.116.069542
This article has not been copyedited and formatted. The final version may differ from this version.

Table 1. Physiological volumes and blood flows used for modeling and simulation of rat data

Blood volume	**mL**	**Blood Flows**	**mL.min^{-1}**
Total blood volume (V_B)[a]	16.2	Hepatic artery (Q_{HA})[h]	3.94
Intestinal blood volume (V_{IB})[b]	1.5	Portal Vein (Q_I)[h]	11.7
Serosal blood ($V_{ser,B}$)= f_Q*V_{IB}	---	Kidney (Q_K)[h]	12.6
Enterocyte blood ($V_{en,B}$)= (1-f_Q)*V_{IB}	---	Highly perfused tissue (Q_{HP})[g]	20.7
Intestinal tissue (V_I)[c]	2.2	Poorly perfused tissue(Q_{PP})[g]	20.4
Serosal tissue (V_{ser}) = f_Q*V_I	---	Adipose tissue (Q_{AD})[g]	6.3
Enterocyte tissue (V_{en})= (1-f_Q)*V_I	---		
Liver blood (V_{LB})[d]	3.24		
Liver tissue (V_L)[e]	6.59		
Kidney blood (V_{KB})[f]	0.31		
Kidney tissue (V_K)[e]	1.31		
Rapidly perfused tissue (heart, lung, brain) (V_{RP})[g]	14.3		
Poorly perfused tissue (muscle, bone, skin) (V_{PP})[g]	210		
Adipose tissue (V_{AD})[g]	21.2		

[a] Obtained from Davies and Morris, 1993
[b] Obtained from Peters, 2008, based on 40% of intestine volume
[c] Obtained from Peters, 2008, based on 60% of intestine volume
[d] Obtained from Everett et al., 1956, based on liver weight of 12.1 g in our study, according to Davies and Morris, 1993
[e] Obtained from Gao et al., 2009, based on 60% of organ volume
[f] Obtained from Everett et al., 1956, based on kidney weight of 2.4 g in our study, according to Davies and Morris, 1993
[g] Obtained from Corley, et al., 2005
[h] Obtained from Gao et al., 2009, based on cardiac output of 89.7 mL·mi^{-1} in our study, according to Davies and Morris, 1993

DMD Fast Forward. Published on April 20, 2016 as DOI: 10.1124/dmd.116.069542
This article has not been copyedited and formatted. The final version may differ from this version.

Table 2. Initial estimates for tissue partitioning coefficients for morphine and MG and estimated according to the method of Rodgers and Rowland (2006; 2007) for PBPK modeling

	Morphine		
	Initial Estimates	**TM**	**SFM**
Blood unbound fraction **(f_B)**	0.654[a] 0.634[b]	0.654	
K_{RP} Partition coefficient for rapid perfused tissue	3.69[c]	2.05 (47.2)[d]	5.03 (38.8)[d]
K_{PP} Partition coefficient for poorly perfused tissue	2.37[c]	1.03 (42.8)[d]	1.16 (60.3)[d]
K_{AD} Partition coefficient for adipose tissue	1.08[c]	0.796 (23.9)[d]	1.63 (20.9)[d]

[a] Doherty and Pang, 2000, using $f_P = 0.89$ and C_B/C_P of 1.08 [$f_B = f_{P/}(C_B/C_P)$]
[b] Mistry and Houston, 1987, using $f_P = 0.85$; C_B/C_P -= 1.34
[c] Calculated according to the method of Rodgers and Rowland, 2006; 2007
[d] Fitted estimates, with %coefficient of variation within brackets

DMD Fast Forward. Published on April 20, 2016 as DOI: 10.1124/dmd.116.069542
This article has not been copyedited and formatted. The final version may differ from this version.

Table 3. Non-compartmental data for M and MG for IV and ID data of morphine sulfate administration to the rat (305 ± 16 g) [a]

PARAMETER	INTRAVENOUS IV (n=4)	INTRADUODENAL ID (n=3)	RATIO ID/IV	*P* value
MORPHINE				
Dose (μmole·kg^{-1})[b]	14.9± 1.6	26.6 ± 0.40	1.79	0.0001*
Rat (g)	299 ± 6	307 ± 12	1.03	0.576
AUC^{M}_{4h} (nM·min^{-1}·nmole dose^{-1})	183 ± 98	39.9±6.0	0.218	0.057
AUC^{M}_{∞} (nM·min^{-1}·nmole dose^{-1})	188 ± 97	43.2±6.1	0.229[c]	0.053
$t^{M}_{1/2\beta}$ (min)	61 ± 12	67 ± 23	1.09	0.691
CL_{tot} (mL·min^{-1})	6.57 ± 3.28			
$A^{M}_{bile,4h}$ (% dose M excreted into bile at 4 h)	0.984 ± 0.508	0.559 ± 0.095	0.568	0.221
$A^{M}_{urine,4h}$ or f_e (% dose M excreted into urine at 4 h)	33.4± 15.1	7.16 ± 2.68	0.215[d]	0.034*
% dose as M into urine and bile (4 h)	34.3 ± 15.4	7.71 ± 2.60	0.225	0.034*
CL_R or $A^{M}_{urine,4h}/AUC^{M}_{4h}$ (mL·min^{-1})	2.21±1.24	1.77±0.45	0.800	0.589
MORPHINE 3-GLUCURONIDE (MG)				
AUC^{MG}_{∞} (nM·min^{-1}·nmole dose^{-1})	26.2±6.8	53±28	2.02	0.114
AUC^{MG}_{∞} (nM·min^{-1}·nmole dose^{-1})	30.3 ± 8.2	60.5 ± 29.0	2.0	0.10
$t^{MG}_{1/2\beta}$ (min)	79 ± 11[#]	72 ± 5	0.911	0.82
$A^{MG}_{bile,4h}$ (%dose of MG excreted into bile at 4 h)	32.8 ± 11.3	58.8 ± 6.1	1.79	0.016*
$A^{MG}_{urine,4h}$ (%dose MG excreted into urine at 4 h)	6.6 ± 3.1	30.7 ± 13.1	4.65	0.015 *
CL^{MG}_{R} or $A^{MG}_{urine,4h} / AUC^{MG}_{4h}$ (mL·min^{-1})	2.63±1.19	6.40±3.29	2.43	0.08
%dose as MG into urine and bile (4 h)	39.5 ± 12.7	89.5 ± 7.0	2.26	0.002*
$A^{MG}_{urine,4h} / A^{MG}_{bile,4h}$	0.212 ± 0.078	0.541 ± 0.274	2.55	0.066
%dose – total recovery in bile & urine (4h)[e]	73.8± 11	97.2± 8.8	1.32	0.030*

[a] values are mean±SD, n=4 for IV and n=3 for intraduodenal (ID) dosing
[b] doses of morphine sulfate, as morphine base equivalent
[c] F_{sys} (based on AUC ratio)
[d] F_{sys} based on urinary data
[e] summed MG and M amounts in urine and bile
[*] $P < 0.05$, unpaired *t* test
[#] $P < 0.05$, paired *t* test, compared to M levels of the same dose and route of administration

DMD Fast Forward. Published on April 20, 2016 as DOI: 10.1124/dmd.116.069542
This article has not been copyedited and formatted. The final version may differ from this version.

Table 4. Fit to 2-compartment model for M and MG (mi) after IV (14.9 ± 1.6 μmole·kg^{-1}) and ID (26.6 ± 0.40 μmole·kg^{-1}) doses of morphine sulfate to the rat (305 ± 16 g) [a]

Parameters	Definition	Individual Fitted Values (CV%)[b]	Population Fitted Values (CV%)[b]
k_{12} (min^{-1})	First-order transfer rate constant between central and peripheral compartments	0.404 (46.9)	0.363 (46.4)
k_{21} (min^{-1})		0.143 (72.9)	0.113 (69.5)
k_{10} (min^{-1})[a]	First-order elimination constant from central compartment	0.0711	0.0735
k_m (min^{-1})	First-order rate constant describing forming MG from M	0.048 (24.3)	0.047 (20.9)
$k_{m,others}$ (min^{-1})	First-order rate constant describing forming other metabolites from M	0.001 (24.1)	0.001 (25.0)
k_{bile} (min^{-1})	First-order rate constant describing biliary secretion of M	0.0001 (31.0)	0.0004 (31.0)
k_{renal} (min^{-1})	First-order rate constant describing renal clearance of M	0.022 (26.8)	0.021 (23.6)
V_1 (mL·kg^{-1})	Volume of distribution of central compartment for M	140 (59.1)	120 (58.0)
k_a (min^{-1})	First-order absorption rate constant of M	0.036 (37.3)	0.034 (35.2)
CL_{tot}	Total clearance of M	9.95	8.82
$g_{mi} = k_m/k_{10}$	Fraction of total morphine clearance responsible for forming MG	0.675	0.642
F_{abs}	Fraction of dose absorbed	0.94 (30.0)	0.95 (24.8)
$k\{mi\}_{bile}$ (min^{-1})	First-order rate constant describing biliary secretion of MG	0.045 (59.1)	0.040 (46.4)
$k\{mi\}_{renal}$ (min^{-1})[c]	First-order rate constant describing renal clearance of MG	0.020 (12.5)	0.020 (12.1)
V{mi} (mL·kg^{-1})	Volume of distribution of metabolite compartment	306 (36.0)	292 (29.8)

[a] calculated based on fitted parameters: $k_{10} = k_m + k_{m,other} + k_{bile} + k_{urine}$
[b] Fitted estimates, with %coefficient of variation expressed within brackets
[c] $k\{mi\} = k\{mi\}_{renal} + k\{mi\}_{bile}$

Table 5: Fitted parameters for the PBPK models, with nested TM or SFM intestinal models, showing SFM is the superior model; values are presented as mean ± (CV%)

Fitted Parameters	**Definition**	**TM**	**SFM**
f_Q	Fraction of Q_I to enterocyte region	1	0.10 (11.7)
k_a (min^{-1})	Absorption rate constant of morphine	0.03 (12.6)	0.028 (7.91)
F_{abs}	Fraction of dose absorbed in gut lumen	0.90 (10.2)	0.92 (10.7)
$f_B^M CL_{in,I}$ ($mL \cdot min^{-1}$)	Net influx clearance of morphine in the intestine	0.821(44.9)	1.38 (49.2)
$f_I^M CL_{ef,I}$ ($mL \cdot min^{-1}$)	Net efflux clearance of M in intestine	5.99 (34.9)	2.60 (39.9)
$f_B^M CL_{in,L}$ ($mL \cdot min^{-1}$)	Net influx clearance of M in liver	15.0 (43.8)	14.5 (17.6)
$f_L^M CL_{ef,L}$ ($mL \cdot min^{-1}$)	Net efflux clearance of M in liver	10.6 (10.0)	5.90 (14.0)
$f_I^M CL_{int,met,I}^{M \rightarrow MG}$ ($mL \cdot min^{-1}$)	Metabolic intrinsic clearance forming MG in intestine	3.14 (34.2)	2.93 (22.9)
$f_I^M CL_{int,sec,I}^{M}$ ($mL \cdot min^{-1}$)	Net intestinal intrinsic secretion clearance for M	1.59 (9.92)	2.09 (11.1)
$f_L^M CL_{int,met,L}^{M \rightarrow MG}$ ($mL \cdot min^{-1}$)	Metabolic intrinsic clearance forming MG in liver	7.43 (16.5)	3.73 (28.3)
$f_L^M CL_{int,met,L}^{M \rightarrow others}$ ($mL \cdot min^{-1}$)	Metabolic intrinsic clearance forming other metabolites in liver	0.35 (12.0)	0.51 (21.4)
$f_L^M CL_{int,sec,L}^{M}$ ($mL \cdot min^{-1}$)	Biliary clearance of morphine	0.06 (12.7)	0.13 (18.8)
$f_B^M CL_R^M$ ($mL \cdot min^{-1}$)	Renal clearance of M	0.91 (54.5)	1.27 (57.8)
CL_R^M ($mL \cdot min^{-1}$)	Renal clearance for M after correcting for f_B^M (Table 2)	1.39	1.94
$f_I^{MG} CL_{ef,I}^{MG}$ ($mL \cdot min^{-1}$)	Efflux clearance for MG in the intestine	4.09 (24.1)	2.97 (4.7)
$f_I^{MG} CL_{int,sec,I}^{MG}$ ($mL \cdot min^{-1}$)	Intestinal intrinsic secretion for MG	0.22 (21.8)	0.35 (11.4)
$f_B^M CL_{in,L}^{MG}$ ($mL \cdot min^{-1}$)	Influx clearance for MG in the liver	1	1
$f_L^{MG} CL_{ef,L}^{MG}$ ($mL \cdot min^{-1}$)	Efflux clearance for MG in the liver	0.04 (62.1)	0.2 (56.8)
$f_L^{MG} CL_{int,sec,L}^{MG}$ ($mL \cdot min^{-1}$)	Biliary clearance of MG	0.29 (38.3)	0.70 (43.5)
$f_B^{MG} CL_R^{MG}$ ($mL \cdot min^{-1}$)	Renal clearance of MG	2.40 (54.5)	0.40 (48.3)
CL_R^{MG} ($mL \cdot min^{-1}$)	Renal clearance for MG after correcting for $f_B^{MG} = 0.98$	3.67	0.613
AIC	Akaike information criteria	317	308

Table 6. Comparison of the goodness-of-fit among the three models

	Two-Compartmental Model	TM-PBPK	SFM-PBPK
Weighted residual sum of squares WRSS	445	419	394
F value	---	vs. two-compartment model 4.31[a]	vs. two-compartment model 7.83[a]
	---	---	vs. TM-PBPK Model 23.0[a]

[a] calculated F score > critical F value of 4.0, suggesting the order of goodness of fit: two-compartment model < TM-PBPK < SFM-PBPK

DMD Fast Forward. Published on April 20, 2016 as DOI: 10.1124/dmd.116.069542
This article has not been copyedited and formatted. The final version may differ from this version.

Table 7. Additional parameters obtained from estimates in Table 5

Parameter	Definition	TM-PBPK	SFM-PBPK
$\frac{f_B^M CL_{in,I}^M}{f_I^M CL_{ef,I}^M}$	Ratio of effective uptake/efflux clearance of M in intestine, or intestine to blood partitioning of unbound morphine	0.137	0.531
$\frac{f_B^M CL_{in,L}^M}{f_L^M CL_{ef,L}^M}$	Ratio of effective uptake/efflux clearance of M in liver, or liver to blood partitioning ratio of unbound morphine	1.42	2.46
F_I	Intestinal availability of M $\frac{CL_{ef,I}^M}{CL_{ef,I}^M + CL_{int,sec,I}^M(1-F_{abs}) + CL_{int,met,I}^{M\to MG}}$ $\frac{f_Q Q_I CL_{ef,I}^M}{f_Q Q_I CL_{ef,I}^M + (f_Q Q_I + f_B^M CL_{in,I}^M)\left[CL_{int,met,I}^{M\to MG} + CL_{int,sec,I}^M(1-F_{abs})\right]}$ [a]	0.654 0.629	0.457 0.282
F_L	Hepatic availability of M $\frac{CL_{ef,L}^M}{CL_{ef,L}^M + CL_{int,met,L}^{M\to MG} + CL_{int,met,L}^{M\to others} + CL_{int,sec,L}^M}$ $\frac{(Q_I + Q_{HA})(CL_{ef,L}^M + CL_{int,sec,L}^M + CL_{int,met,L}^{M\to MG} + CL_{int,met,L}^{M\to others})}{(Q_I + Q_{HA})(CL_{ef,L}^M + CL_{int,sec,L}^M + CL_{int,met,L}^{M\to MG} + CL_{int,met,L}^{M\to others}) + f_B^M CL_{in,L}^M (CL_{int,sec,L}^M + CL_{int,met,L}^{M\to MG} + CL_{int,met,L}^{M\to others})}$ [a]	0.574 0.710	0.574 0.717
$F_{sys} = F_{abs} * F_I * F_L$	Systemic bioavailability: $F_{abs} * \frac{CL_{ef,I}^M}{CL_{ef,I}^M + CL_{int,sec,I}^M(1-F_{abs}) + CL_{int,met,I}^{M\to MG}} * \frac{CL_{ef,L}^M}{CL_{ef,L}^M + CL_{int,met,L}^{M\to MG} + CL_{int,met,L}^{M\to others} + CL_{int,sec,L}^M}$ $F_{abs} \frac{f_Q Q_I CL_{ef,I}^M}{f_Q Q_I CL_{ef,I}^M + (f_Q Q_I + f_B^M CL_{in,I}^M)\left[CL_{int,met,I}^{M\to MG} + CL_{int,sec,I}^M(1-F_{abs})\right]}$ $* \frac{(Q_I + Q_{HA})(CL_{ef,L}^M + CL_{int,sec,L}^M + CL_{int,met,L}^{M\to MG} + CL_{int,met,L}^{M\to others})}{(Q_I + Q_{HA})(CL_{ef,L}^M + CL_{int,sec,L}^M + CL_{int,met,L}^{M\to MG} + CL_{int,met,L}^{M\to others}) + f_B^M CL_{in,L}^M (CL_{int,sec,L}^M + CL_{int,met,L}^{M\to MG} + CL_{int,met,L}^{M\to others})}$	0.334 0.402	0.242 0.186
$F\{mi\}_I$	Intestinal availability of MG $\frac{CL_{ef,I}^{MG}}{CL_{ef,I}^{MG} + CL_{int,sec,I}^{MG}}$	0.95	0.89
$F\{mi\}_L$	Hepatic availability of MG $\frac{CL_{ef,L}^{MG}}{CL_{ef,L}^{MG} + CL_{int,sec,L}^{MG}}$	0.11	0.22
h_{mi}	Fraction of hepatic clearance of M forming MG $\frac{CL_{int,met,L}^{M\to MG}}{CL_{int,met,L}^{M\to MG} + CL_{int,met,L}^{M\to others} + CL_{int,sec,L}^M}$	0.948	0.854
$g_{mi} = (1-f_e)h_{mi}$ [b]	Fraction of total body clearance of M forming MG (f_e = 0.334 from Table 3)	0.631	0.569
$\frac{v_I}{v_I + v_L}$ [c]	Fractional contribution of intestine to intestinal-liver removal	0.460 0.570 [e]	0.093 0.171 [e]
$\frac{v_L}{v_I + v_L}$ [d]	Fractional contribution of liver to intestinal-liver removal	0.540 0.430 [e]	0.907 0.829 [e]

[a] equations from Pang and Chow (2012)

[b] based on definition of Pang and Kwan (1983)

[c] calculated based on equations from Pang and Chow 2012: $\frac{v_I}{v_I + v_L} = \frac{f_Q Q_I (1-F_I)}{f_Q Q_I (1-F_I) + E_L \left\langle Q_I \left[f_Q F_I + (1-f_Q) \right] + Q_{HA} \right\rangle}$

[d] calculated based on equations from Pang and Chow 2012: $\frac{v_L}{v_I + v_L} = \frac{E_L \left\langle Q_I \left[f_Q F_I + (1-f_Q) \right] + Q_{HA} \right\rangle}{f_Q Q_I (1-F_I) + E_L \left\langle Q_I \left[f_Q F_I + (1-f_Q) \right] + Q_{HA} \right\rangle}$

[e] F_I and F_L values, based on equations from Pang and Chow, 2012.

DMD Fast Forward. Published on April 20, 2016 as DOI: 10.1124/dmd.116.069542
This article has not been copyedited and formatted. The final version may differ from this version.

Table 8. Discrimination between the TM-PBPK and SFM-PBPK models by the MG urine/bile ratio for ID/IV, demonstrating the route-dependent intestinal glucuronidation of M

	MG **Ratio of MG in (urine/bile)**					
	intraduodenal (ID) Dosing		**Intravenous (IV) Dosing**		**ID/IV Dosing**	
	4 h	**∞**	**4 h**	**∞**	**4 h**	**∞**
Observed	**0.541**	**--- [a]**	**0.212**	**--- [a]**	**2.55**	**--- [a]**
Compartmental Modeling	0.485	0.485	0.485	0.485	1.0	1.0
TM-PBPK	0.131	0.131	0.131	0.131	1.0	1.0
SFM-PBPK	0.453	0.444	0.175	0.179	2.59	2.47

[a] not measured

Figure 1

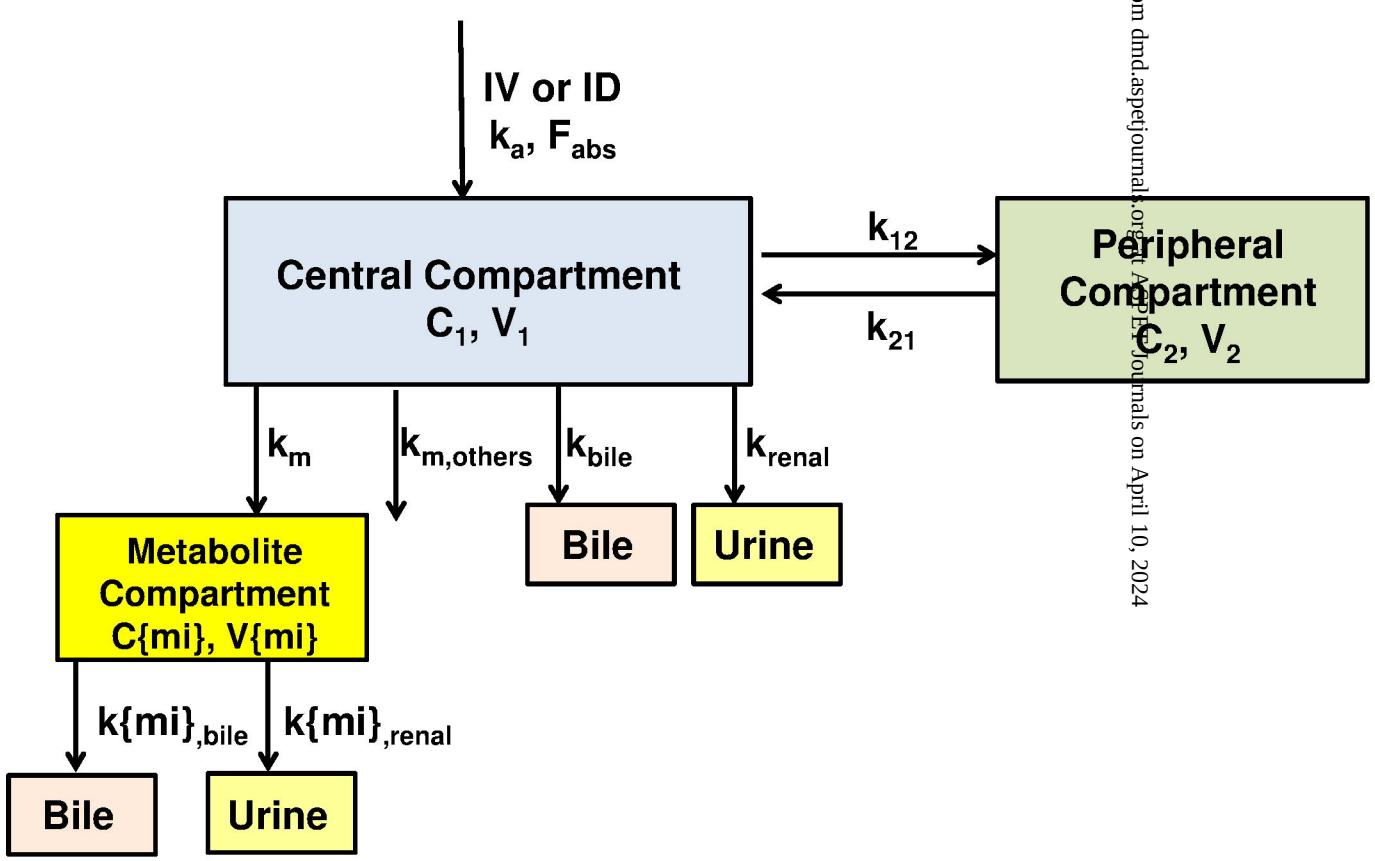

DMD Fast Forward. Published on April 20, 2016 as DOI: 10.1124/dmd.116.069542
This article has not been copyedited and formatted. The final version may differ from this version.

Figure 2

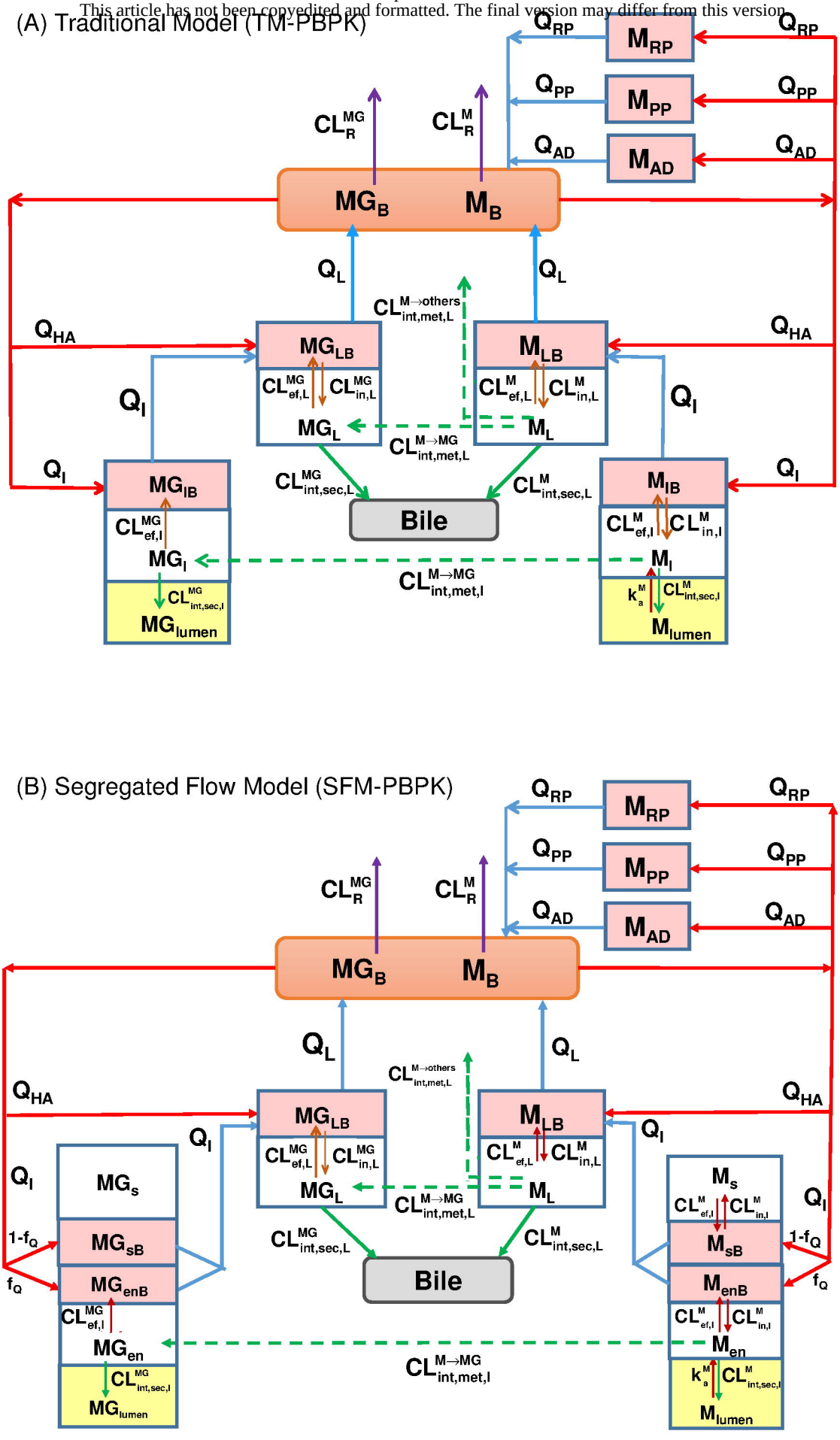

DMD Fast Forward. Published on April 20, 2016 as DOI: 10.1124/dmd.116.069542
This article has not been copyedited and formatted. The final version may differ from this version.

Figure 3

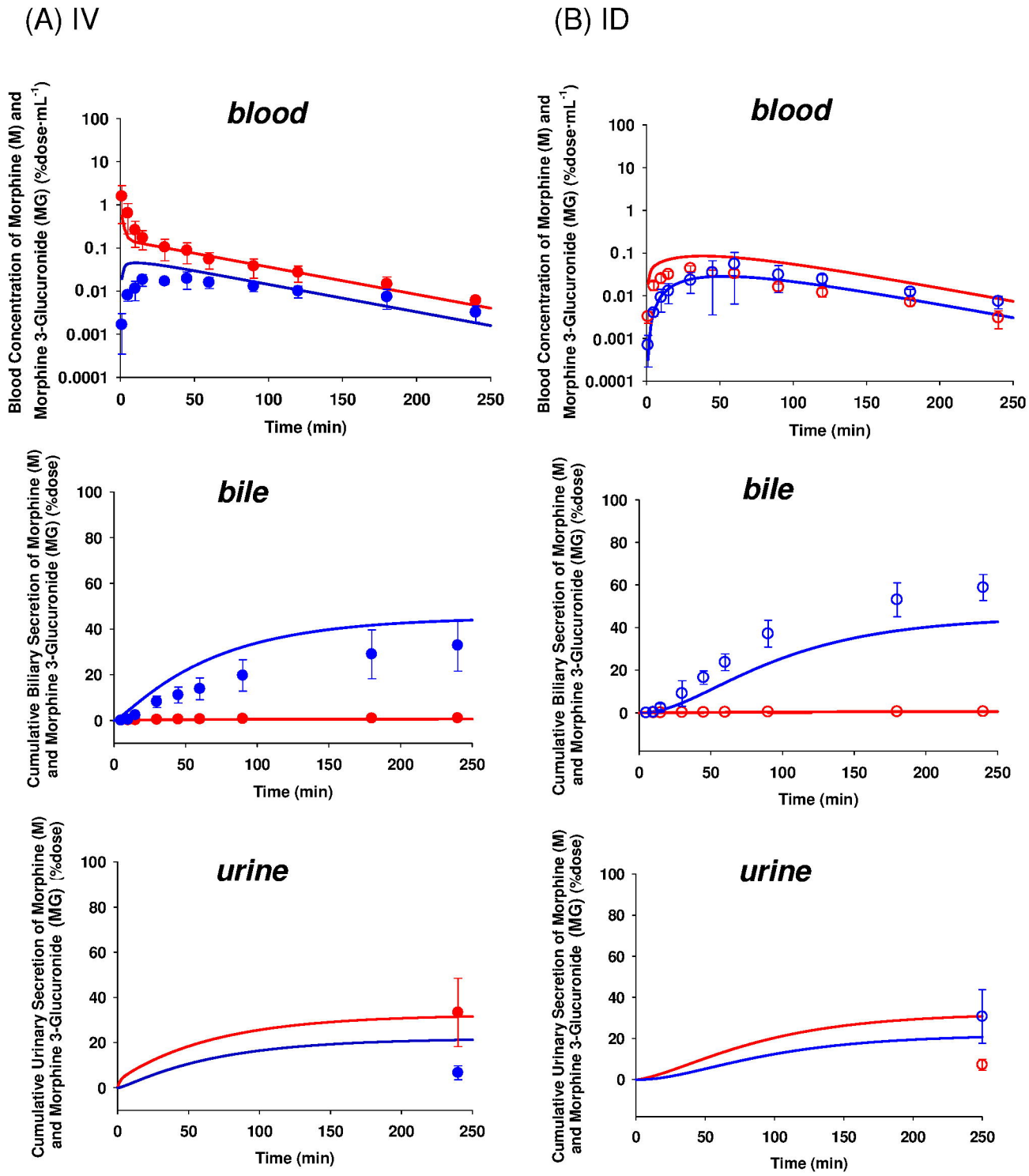

DMD Fast Forward. Published on April 20, 2016 as DOI: 10.1124/dmd.116.069542
This article has not been copyedited and formatted. The final version may differ from this version.

Figure 4

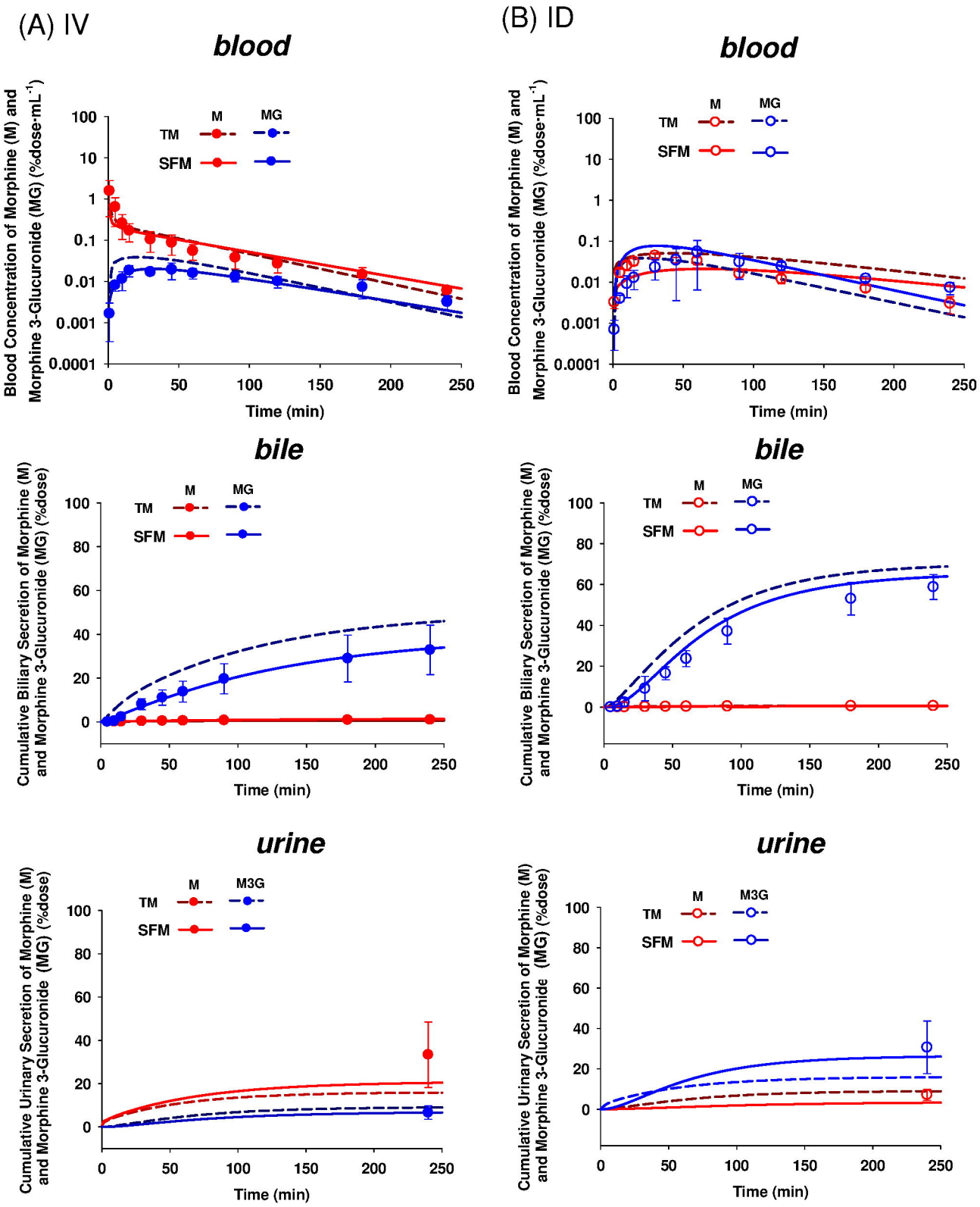

DMD Fast Forward. Published on April 20, 2016 as DOI: 10.1124/dmd.116.069542
This article has not been copyedited and formatted. The final version may differ from this version.

Figure 5

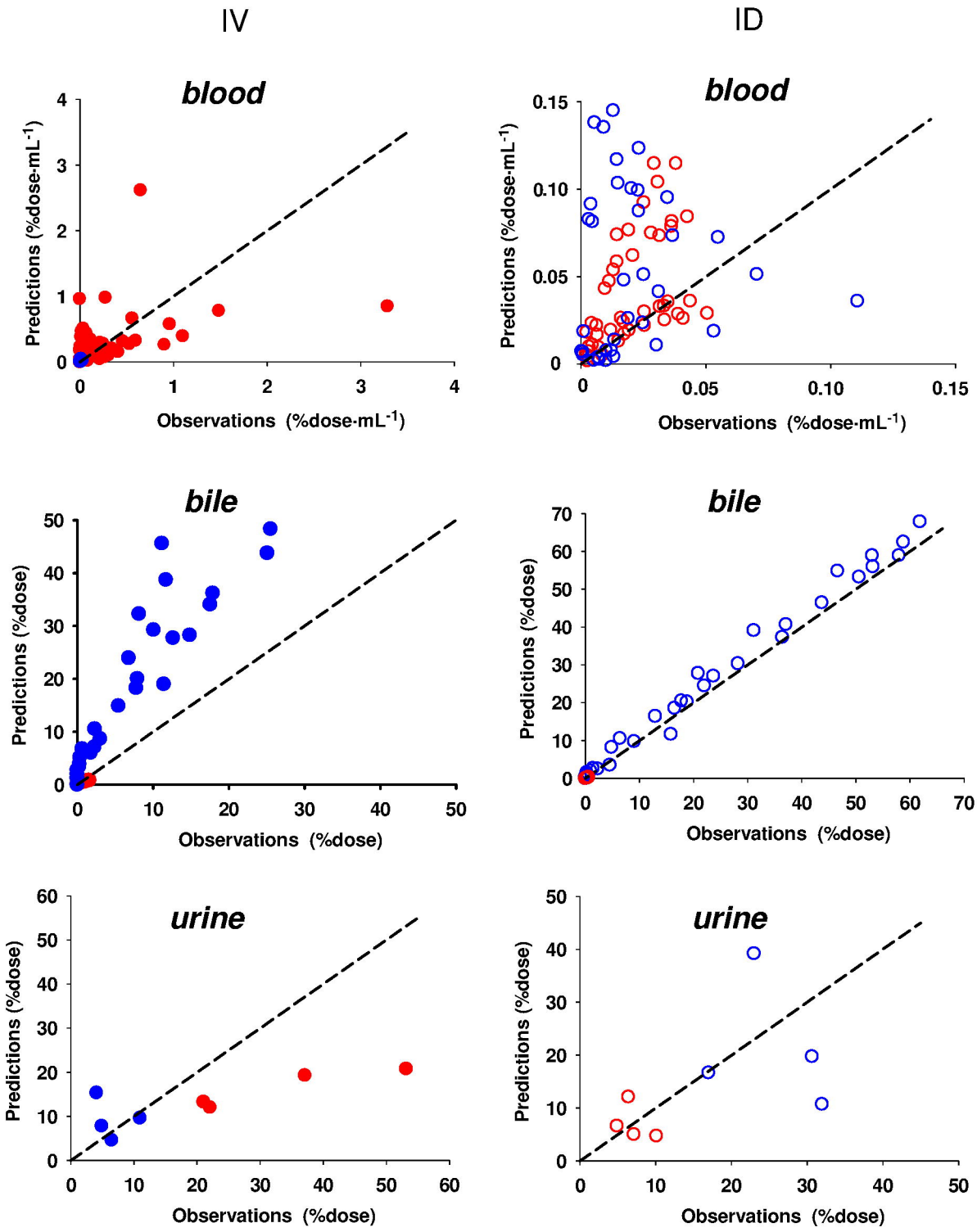

DMD Fast Forward. Published on April 20, 2016 as DOI: 10.1124/dmd.116.069542
This article has not been copyedited and formatted. The final version may differ from this version.

Figure 6